═══REVIEW COMMONS MANUSCRIPT═══

IMPORTANT:

- Manuscripts submitted to Review Commons are peer reviewed in a journal-agnostic way.
- Upon transfer of the peer reviewed preprint to a journal, the referee reports will be available in full to the handling editor.
- The identity of the referees will NOT be communicated to the authors unless the reviewers choose to sign their report.
- The identity of the referee will be confidentially disclosed to any affiliate journals to which the manuscript is transferred.

GUIDELINES:

- For reviewers: https://www.reviewcommons.org/reviewers
- For authors: https://www.reviewcommons.org/authors

CONTACT:

The Review Commons office can be contacted directly at: office@reviewcommons.org

Autosomal Allelic Inactivation: Variable Replication and Dosage Sensitivity

Michael B. Heskett[1], Athanasios E. Vouzas[2], Brian Johnstone[3], Krister P. Freese[4], Phillip A. Yates[5], Philip F. Copenhaver[6], Paul T. Spellman[1], David M. Gilbert[2], Mathew J. Thayer[5,*].

[1]Division of Hematology Oncology
Departments of Medicine and Human Genetics
David Geffen School of Medicine
University of California, Los Angeles

[2]San Diego Biomedical Research Institute
3525 John Hopkins Court
San Diego, CA 92121

[3]Shriners Hospitals for Children—Portland
3101 SW Sam Jackson Park Rd,
Portland, Oregon, 97239

[4] Department of Orthopedics and Rehabilitation
[5]Department of Chemical Physiology and Biochemistry
[6]Department of Cell, Developmental and Cancer Biology
Oregon Health & Science University
3181 S. W. Sam Jackson Park Road
Portland, Oregon 97239

***Corresponding author.**

ORCID: 0000-0001-6483-1661

TEL: (503) 494-2447

FAX: (503) 494-7368

Email:thayerm@ohsu.edu

Abstract

Autosomal monoallelic gene expression and asynchronous replication between alleles are well-established features of imprinted genes and genes regulated by allelic exclusion. Inactivation/Stability Centers (I/SCs) are recently described autosomal loci that exhibit epigenetic regulation of allelic expression and replication timing, with differences that can be comparable to those observed between the active and inactive X chromosomes [1]. Here we characterize hundreds of autosomal loci with allele-specific epigenetic regulation of replication timing and gene expression, defining them as I/SCs. I/SCs are approximately 1 megabase in size and can contain both protein-coding and noncoding genes. In different single cell derived clones, these genes may be expressed from a single allele, the opposite allele, both alleles, or not expressed at all. This stochastic, yet mitotically stable, pattern indicates that the choice of which allele is expressed is independent of parent of origin and independent of the expression status of the other allele. Similarly, alleles within I/SCs show varying replication timing, either earlier or later, that is also independent of the other allele. Additionally, we find corresponding I/SCs in the mouse genome that display conserved synteny with human I/SCs. This allele-restricted regulation creates extensive cellular mosaicism through a stable epigenetic mechanism. This mosaicism impacts numerous dosage-sensitive genes associated with human diseases such as Parkinson, epilepsy, deafness, and impaired intellectual development.

Introduction:

The relationship between monoallelic expression and asynchronous replication between alleles of autosomal genes, exemplified by genes subject to genomic imprinting or allelic exclusion, has been the focus of extensive research for over three decades [2-4]. In recent work, we employed haplotype-phased RNA expression and replication timing assays on multiple single-cell-derived Lymphoblastoid Cell Line (LCL) clones from two unrelated individuals to identify loci exhibiting allele-restricted expression and replication timing [1]. This clonal, allele-specific analysis across autosomes revealed an unexpected genomic feature at approximately 200 loci, exhibiting allele-restricted gene expression (including random monoallelic expression); and variable replication timing (including asynchronous replication between alleles). The magnitude of allelic differences in expression and replication timing observed in some of the clones was comparable to the large differences detected between the active and inactive X chromosomes**.** We have named these autosomal loci Inactivation/Stability Centers (I/SCs) [1,5-7].

I/SCs can encompass both coding and noncoding genes that may be expressed from a single allele in some clones, expressed from the opposite allele in other clones, biallelically expressed in other clones, or silent on both alleles in yet other clones. This pattern of allele-restricted expression indicates that each allele independently adopts either an expressed or silent state. Importantly, because these expression states are mitotically stable, allele-autonomous, and independent of parental origin, we refer to the choice of the expressed allele as stochastic [1]. To describe this phenomenon, we and others have used the term Allelic Expression Imbalance (AEI) to refer to the stochastic nature of autosomal random monoallelic expression [1,8-11]. Additionally, the replication timing profiles on autosomes are highly variable and clone-specific, exhibiting both

synchronous and asynchronous patterns in different clones. We refer to this as Variable Epigenetic Replication Timing (VERT) [1].

Random monoallelic expression in the olfactory, immune, and central nervous systems is well established and plays a critical role in generating cell-specific identities [12-14]. However, increasing evidence indicates that autosomal genes outside these systems also exhibit allele-specific expression, suggesting that AEI plays a broader role across diverse cell types [4,13]. The functional diversity of these genes implies that AEI contributes to a broad array of cellular processes and is not limited to specialized systems.

In the present study, we aimed to determine whether I/SCs could be detected in the genomes of clonal populations of human primary cells derived from a tissue distinct from those previously examined. To this end, we employed articular cartilage progenitor (ACP) cells as a second model system [15]. ACP cells are non-transformed yet are particularly well-suited for clonal analysis due to several advantages: 1) they can be readily isolated from amputated tissue of patients with polydactyly, 2) they exhibit high proliferative capacity, and 3) they can be efficiently expanded from single cells [16]. We identify an additional 163 VERT regions in the human genome, increasing the total number of potential I/SCs to 363, which collectively cover approximately 12% of the human genome. In addition, we found that many previously reported "random monoallelic" genes, including those encoding olfactory and vomeronasal receptors[3,17], antigen receptors[18], and homophilic cell adhesion proteins[12], are located within VERT regions. Our findings confirm that these well-established "random monoallelic" genes reside within genomic loci that exhibit the epigenetic hallmarks, namely allele-restricted expression and variable replication timing, that define I/SCs.

The relationship between genotype and phenotype is central to understanding human genetic disease. While most loss-of-function mutations are recessive, indicating that a single normal allele is sufficient for typical function, dominantly inherited disorders often result from gain-of-function mutations**.** However, a significant fraction of dominant diseases arises through haploinsufficiency (i.e. heterozygous for a loss of function mutation), where a single functional allele fails to maintain normal physiology. Although haploinsufficiency may affect up to 40% of human genes [19-21], the underlying molecular mechanisms remain poorly understood. Current models suggest that insufficient gene dosage may arise from a lack of redundancy, critical expression thresholds, stoichiometric imbalances, or toxicity associated with a lack of overexpression buffering [22-25]. In contrast, insights from X-linked disease inheritance illustrate how cellular mosaicism and cellular selection can shape phenotypic outcomes: in XX individuals, differences in the survival or expansion of cells expressing either the wild-type or mutant alleles can influence whether a disease manifests as recessive or dominant [21,26,27].

The magnitude of AEI is often quantified using allelic expression ratios, which represent the proportion of transcripts derived from each allele. Importantly, recent findings have demonstrated that even modest allelic expression biases can have functional consequences, particularly in disease contexts. One recent study directly linked small but stable AEI to variable clinical outcomes among individuals carrying the same pathogenic mutation, underscoring AEI as a potential modulator of disease expressivity [28]. These observations highlight the importance of considering AEI as a disease modifier that may shape phenotypic diversity and influence the penetrance of genetic disorders.

Here, we demonstrate that numerous genes implicated in autosomal human genetic diseases, such as Parkinson (DNAJC6, LRRK2 and SNCA), epilepsy (SCN1A, GABR1, and SAMD12), deafness (ATP11A, EPS8, and MYO6), and neurodevelopmental disorders (KCNA1, RETREG1, ROBO1, and TIAM1), are located within VERT regions and display AEI. Furthermore, mapping I/SCs across all autosomes reveals 87 known dominantly inherited single-gene disorders that map within VERT regions, where loss of function mutations in most of these genes result in haploinsufficiency [29]. We propose that epigenetically regulated stochastic AEI can contribute to pathogenic phenotypes in heterozygous individuals by either reducing the number of functional cells below a critical disease threshold, akin to X linked dominant disorders, or by disrupting the normal mosaicism of gene expression within disease-relevant tissues.

Results

Here we employed articular cartilage progenitor (ACP) cells[15], as a distinct cell type from those from our previous studies, as a second model system to identify I/SCs. For this analysis, we isolated ACP cells from amputated digits of patients with polydactyly. In addition, we sequenced genomic DNA from the parents of the patients with polydactyly to generate phased genomes of the ACP cells. We analyzed two sets of ACP clones isolated from two unrelated individuals, one female (ACP7) and one male (ACP6), for haplotype-phased Repliseq and RNAseq (Fig. 1b). Analysis of the female ACP7 clones allowed us to establish the statistical parameters for the assignment of VERT and AEI present in the ACP clones by directly comparing the magnitude of autosomal allele-specific replication timing and RNA expression to that of the active and inactive X chromosomes present in each clone (Fig. 1c; and see Supplementary Tables

1, 2 and 3). Taken together the combined VERT and AEI analysis allowed us to characterize additional I/SCs in the human genome. An illustration of a hypothetical I/SC, with the region of VERT shaded in gray and the expression of coding and noncoding genes indicated as stippled or smooth rectangles, respectively, is shown in Figure 1d.

To identify genomic regions with epigenetic variation between alleles**,** we calculated the standard deviation (SD) of replication timing across alleles for each 250 kb genomic window. Windows with an SD value ≥ 2.5 standard deviations above the genome-wide median were classified as outliers. This analysis identified 163 additional VERT regions (Supplementary Table 1). Figure 1e illustrates this analysis for both ACP (ACP6 and ACP7) and LCL (EB3-2 and GM12878) clones on Chromosome 1, where windows are indicated as gray circles and outliers indicted in different colors.

To detect coding genes with AEI in ACP clones, we defined AEI as differential expression between alleles using recently established criteria [1,28]. Genes were considered AEI-positive if they exhibited ≥80% allelic imbalance (AEI ≥ 0.80 or ≤ 0.20) with FDR $\leq$ 0.05 in at least one clone. Additional analyses using more stringent thresholds (AEI ≥ 0.90 or ≥ 0.95) are provided in Supplementary Table 2. To exclude imprinted genes and effects due to genetic polymorphisms (i.e. expression Quantitative Trait Loci, eQTL[30]) we required that each AEI gene also be biallelically expressed (AEI < 0.70) in at least one clone from the same individual with ≥ 20 informative reads. Using these criteria, we identified 256 (2.4% of expressed genes) autosomal coding genes exhibiting AEI across the two ACP clone sets (Supplementary Table 2).

In addition, we also sought to identify AEI of extremely long noncoding RNAs (i.e. ASAR lincRNAs [1,5,7,31]) expressed in the ACP clones. For this analysis we refer to regions of the genome with >50 kb of contiguous transcription of noncoding DNA as Transcribed Loci (TL) [1]. Using the same criteria used for the coding genes described above, we identified 23 TLs exhibiting AEI across the two ACP clone sets (Supplementary Table 3).

Allelic Expression Imbalance and Variable Epigenetic Replication Timing define Inactivation/Stability Centers.

By integrating the location of genes exhibiting AEI with genomic regions displaying VERT, we identified overlapping loci that define I/SCs**.** Figures 1f and 1g illustrate a representative I/SC located on chromosome 1 at approximately 240 Mb (marked by an arrow in Fig. 1e). Notably, VERT was detected at this locus across both sets of ACP clones (Fig. 1f and 1g). Figure 1h presents the corresponding UCSC Genome Browser view of this locus, with genes showing AEI marked by asterisks (see Supplemental Table 2). Additional examples of I/SCs located on chromosomes 18, 6 and 9 are shown in Figure 2.

One of the primary objectives of this study was to determine whether different tissues utilize distinct sets of I/SCs, as might be expected given that different cell types express unique gene repertoires that could be subject to AEI. To explore this, we performed hierarchical clustering analysis of the VERT regions identified in the two sets of ACP clones and the two sets of LCL clones**.** Figure 1i shows this analysis and reveals tissue-specific patterns with a relatively small degree of overlap in VERT regions across

the two tissue types: ACP6 clones share more VERT regions with ACP7 clones than with either LCL clone sets, and the reverse is true for the LCL clones. These findings indicate that while some I/SCs are shared across tissues, there is a large component of tissue-specific epigenetic regulation of allelic replication timing.

At the molecular level, stochastic monoallelic expression contributes to cellular individuality and introduces functional variability among individual cells within complex biological systems [12-14]. This mechanism is particularly well characterized in the olfactory, immune, and central nervous systems, where the expression of diverse receptor-type molecules through random monoallelic expression underlies cell-specific functional identities. To further investigate the functional characteristics of protein-coding genes located within I/SCs, we annotated the genes residing within the VERT regions identified across all four clonal datasets (ACP clones: ACP6 and ACP7; and LCL clones: EB3-2, and GM12878; see Supplementary Table 4). To assess whether these genes are functionally related, we performed a Gene Ontology (GO) enrichment analysis. This analysis revealed a significant enrichment for genes involved in plasma membrane localization, cell-cell adhesion and neurodevelopmental processes, the most significant hits for each set of clones is presented in Figure 1k (see full details in Supplementary Table 5). This analysis suggests that I/SC-associated epigenetic regulation may play a broader role in the establishment of cellular identity and tissue organization particularly in the nervous system.

Gene clusters with AEI map to VERT regions.

In the olfactory, immune, and central nervous systems, random monoallelic expression of gene family members, often organized in genomic clusters, plays a key

role in establishing cell-specific identities [12-14]. Consistent with these observations, we found that VERT regions frequently coincide with gene clusters in the human genome (Table 1). For example, Figures 3a and 3b highlight a cluster of 11 olfactory receptor (OR) genes located on human chromosome 19 at approximately 15 Mb. This region also harbors a cluster of Cytochrome P450 (CYP4F family, n = 6) genes. The interspersed genomic arrangement of the CYP4F genes among the OR genes, indicates that both gene families reside within the same I/SC and therefore both may be subject to AEI.

A second example of a gene cluster is shown in Figures 3c and 3d, where the major histocompatibility complex (MHC), comprising 16 HLA genes (which are known to be subject to AEI [28,32]), lies within a VERT region. Notably, this locus also contains a cluster of Lymphocyte Antigen 6 genes (LY6G family, n = 6), which are interspersed among the HLA genes. This genome organization indicates that the LY6G genes, like their neighboring HLA genes, are within the same I/SC and suggests that they too may be subject to stochastic allelic expression**.**

Mapping mouse VERTs identifies known AEI gene clusters and syntenic I/SCs.

Much of our current understanding of stochastic autosomal allelic expression is derived from studies conducted in the mouse [4,9-11,17,18,33-40]. To assess whether VERT regions could be identified at expected loci in the mouse genome, specifically at sites of known AEI, we analyzed previously published Repli-seq data from mouse pre-B cell clones reported by Blumenfeld et al [41]. This analysis revealed 117 loci in the mouse genome that display VERT (Supplemental Table 6).

Consistent with our findings in the human genome, the VERT regions detected in the mouse genome frequently overlap with gene clusters, including 5 olfactory receptor gene clusters located on four different autosomes (Table 1). Figure 4 presents three examples: two olfactory receptor (Or) gene clusters on mouse chromosome 2 (Figs. 4a–4c) and the protocadherin (Pcdh) gene cluster, which is known to generate cellular individuality in the central nervous system through stochastic expression of different Pcdh family members [12,42], located on mouse chromosome 18 (Figs. 4d–4e). In addition to the gene clusters with VERT, we also detected immunoglobulin and T cell receptor gene loci with VERT. As detailed in Supplemental Figure 1, we detected VERT at the T cell receptor alpha (Tra) locus on mouse chromosome 14 at approximately 54 Mb. One striking feature of this locus is that it also contains an olfactory receptor cluster, containing 37 Or genes, and a vomeronasal receptor gene (Vmn2r88). All of these multigene families are documented sites of AEI [3,12,17,42,43], highlighting the genomic organization and conservation of I/SC-associated regulation at known AEI genes in the mouse. Gene Ontology analysis of the mouse genes located within these regions showed significant enrichment for biological processes related to the plasma membrane and cell-cell adhesion (Fig. 1k), which is consistent with the human VERT gene dataset and reinforces the conservation of this regulatory mechanism across species.

Previous studies analyzed a relatively small number of mouse AEI genes to model their human counterparts with respect to autosomal-dominant disorders [38,44]. To further investigate the conservation of I/SC regulation between the human and mouse genomes, we identified VERT regions that map to syntenic loci across the two species. This analysis revealed 21 loci where VERT is detected in both genomes, as detailed in

Table 2. Figure 5 presents three representative examples of syntenic VERT regions: two loci on the short arm of human chromosome 5 with corresponding regions on mouse chromosome 15 (Figs. 5a–5g), and a third locus on human chromosome 16 with its syntenic region on mouse chromosome 16 (Figs. 5h–5k). Additional examples of syntenic loci showing AEI and/or VERT, including mouse App (see Gimelbrant et al. [45] for AEI of human APP), Mocos and Fhod3 (See Fig. 2A for VERT and AEI of human MOCOS and FHOD3), and a cluster of 5 sodium channel genes, Scn1a, Scn2a, Scn3a, Scn7a and Scn9a (see Fig. 6a-c below for VERT and AEI of the syntenic human SCN gene cluster) are shown in Supplemental Figure 2.

We point out that many of the mouse genes that are located within VERT regions are associated with various human genetic diseases (Supplemental Table 7). One of the loci highlighted in Figure 5a-5d labeled "hi", exhibits both VERT and AEI (Fig. 5c and [1]), affecting the protein-coding gene SEMA5A, a gene implicated in autism and neurodevelopmental disorders [46-48]. Notably, this locus also contains a syntenic pair of taste receptor genes: TAS2R1 in humans and Tas2r119 in mice. These genes are part of the taste receptor family, which are known to harbor chromatin marks characteristic of AEI-regulated loci [49]. Consistent with this observation, we also detected VERT at a taste receptor gene cluster (Tas2r) on mouse chromosome 6 (Table 1).

A second example of synteny is shown in Figure 5f-5g, where human RETREG1 and mouse Retreg1 are located within VERT regions. Human RETREG1 is a known AEI gene [45], and mutations in RETREG1 cause sensory and autonomic neuropathy [29]. A third example is shown in Figure 5h-5k, where both human GRIN2A and mouse Grin2a are located within VERT regions, and loss of function mutations in GRIN2A are known to cause autosomal dominant (i.e. haploinsufficiency) epilepsy [29,50]. These

findings indicate that I/SC-associated epigenetic regulation is conserved across species, affects functionally related gene families, and may influence human genetic disease inheritance patterns (see below).

Neurodevelopmental disease genes map to I/SCs.

To further investigate the relationship between I/SC regulation and human disease genes, we annotated the human protein-coding genes located within VERT regions (see Supplemental Table 4). This analysis identified 979 genes overlapping VERT regions, of which 272 are associated with single-gene disorders according to the OMIM database [29]. Among these genes, 155 are linked to autosomal recessive diseases**,** 87 to autosomal dominant diseases**,** and 30 exhibit both dominant and recessive inheritance patterns (Supplemental Table 8). Consistent with our GO analysis, which revealed an enrichment for neurodevelopmental processes (see Fig. 1k), we found that various neurodevelopmental disease genes were prominently represented among the disease-associated genes (Table 3). Moreover, it was not unexpected to observe gene clusters associated with neurodevelopmental disorders residing within VERT regions. For example, Figures 6a–6c depict the location**,** I/SC profile**,** and genomic organization of a cluster of sodium channel genes (SCN family, n = 5). Mutations in SCN1A, SCN2A, SCN3A, and SCN9A genes are known to cause autosomal dominant developmental and epileptic encephalopathies, with haploinsufficiency as a primary mechanism (Table 3 and [29,51,52]). We also note that the syntenic locus in the mouse displays VERT, with the 5 syntenic mouse Scn genes residing within a VERT region on mouse chromosome 2 (Supplementary Fig. 2e-2f).

A second example of a cluster of epilepsy disease genes is shown in Figures 6d–6e, where four members of the gamma-aminobutyric acid type A receptor gene family (GABR family, n = 4) reside adjacent to a VERT region; notably, GABRA1 displays AEI (Fig. 6e, and Supplementary Table 2), and mutations in GABRA1, GABRB2, and GABRG2 cause autosomal dominant developmental and epileptic encephalopathies [29,53,54]. We also note that a second GABR gene cluster (n = 4), where GABRA2 and GABRB1 are also associated with autosomal dominant developmental and epileptic encephalopathies, is adjacent to a VERT region on chromosome 4 (see Table 1). Two additional examples are shown in Figures 6g–6j, where OXR1 and SAMD12 are located in different VERT regions on chromosome 8, and mutations in each result in autosomal dominant epilepsy [29].

Another prominent group of human disease genes located within I/SCs are those associated with Parkinson disease (Table 3). As shown in Figure 7, four well-characterized Parkinson disease genes, SNCA, LRRK2, DNAJC6, and PARKN, are situated within or adjacent to VERT regions. Importantly, both SNCA and LRRK2 were among the first genes identified as displaying AEI in the study by Gimelbrant et al. in 2007 [45]. In our own dataset, we found that DNAJC6 exhibits AEI in LCL clones [1]. We also highlight that JAK1, a gene involved in immune signaling, lies within the same I/SC as DNAJC6 (Fig. 7f). JAK1 is a known AEI gene [55,56], and mutations in JAK1 cause autosomal dominant autoinflammation, immune dysregulation, and eosinophilia (AIIDE). A recent study indicated that AEI of wild-type and mutant JAK1 alleles correlates with variable disease penetrance [28].

Taken together, these findings underscore the role of I/SCs in regulating disease-relevant gene clusters and emphasize their conservation, synteny, and functional

relevance in both neurological and immune-related disorders. These examples highlight how stochastic epigenetic regulation within I/SCs contributes to phenotypic variability and disease risk.

Discussion:

The co-occurrence of random monoallelic expression and asynchronous replication between alleles of autosomal genes is well documented [2-4], yet its developmental potential and contribution to human disease have not been systematically investigated. In this study, we expand on the discovery and characterization of Inactivation/Stability Centers (I/SCs), autosomal loci marked by AEI and VERT, by identifying an additional 163 VERT regions using clonal lines of primary ACP cells. This brings the total number of I/SCs to 363, covering approximately 12% of the human genome.

To assess the evolutionary conservation of I/SC regulation, we analyzed replication timing data from mouse pre-B cell clones, identifying 117 mouse VERT loci. Many of these regions overlap with known mouse AEI genes and gene clusters including olfactory, vomeronasal, and antigen receptors as well as protocadherin gene families. Notably, we identified 21 syntenic VERT regions shared between human and mouse genomes. These findings reinforce and extend previous observations indicating a high degree of conservation of AEI genes [4] and suggest that I/SCs are a fundamental and widespread feature of autosomal epigenetic regulation in mammals.

I/SC regulation imparts cell-type specific and tissue-relevant variation

Our clonal analysis of ACP and LCL cells, combined with haplotype-phased replication timing and expression profiling, enabled us to identify tissue-specific I/SCs, while also confirming a subset of I/SCs that are shared across tissues and conserved between species**.** These findings support a dual regulatory model in which certain I/SCs may serve ubiquitous functions and are utilized broadly across cell types, whereas others are selectively engaged based on the gene expression program and functional requirements of a given tissue. This model is supported by hierarchical clustering analysis of VERT regions, which showed greater overlap within tissue type (ACP6 vs. ACP7; EB3-2 vs. GM12878) than between tissues, suggesting that I/SC activity is tightly linked to cellular identity.

Importantly, we identified 68 VERT regions shared across two or more clonal sets, representing high-confidence I/SCs that likely reflect core regulatory regions active across individuals and cell types (Fig. 1i). As detailed in Supplemental Table 1, we also identified VERT regions detected exclusively in single clone sets. These private VERT regions may reflect inter-individual variability in epigenetic regulation, context-dependent I/SC usage, but more likely reflect a limitation of sampling—i.e., regions that would be detected in additional clones if a larger number were analyzed. Thus, while our findings provide strong support for both shared and tissue specific I/SCs, they also underscore the importance of clone number and diversity in defining the full landscape of autosomal epigenetic regulation.

In the context of development, AEI introduces stochastic variability in gene dosage across clonal populations, contributing to cellular heterogeneity during lineage specification and tissue formation. Such heterogeneity could serve as a substrate for cellular selection, enabling the developing tissue to fine-tune function or respond

adaptively to environmental cues. This model aligns with observations that AEI often affects genes involved in cell adhesion, signal transduction, and neurodevelopment, where even small variations in expression levels could significantly impact cell fate and connectivity.

At the molecular level, I/SCs contribute to cellular individuality by enabling stochastic monoallelic expression of specific genes. This mechanism is particularly critical in biological systems that require diversity at the single-cell level, such as the olfactory, vomeronasal, immune, and nervous systems. Consistent with this, many I/SCs coincide with gene clusters, including olfactory, vomeronasal, and antigen receptor genes, as well as HLA and protocadherin genes, all of which are known to undergo stochastic monoallelic expression. We identified numerous additional gene clusters residing within I/SCs, suggesting that these other gene families may also participate in tissue mosaicism and/or cellular individuality. Our current model proposes that I/SC regulation is integral to tissue development, where stochastic, epigenetically driven allelic regulation introduces phenotypic variability among cells. This variability may promote functional diversity and selective advantage during development. Under this model, each tissue would engage a distinct but partially overlapping set of I/SC-regulated genes, aligned with its unique transcriptional and functional requirements. This framework positions I/SCs as key players in promoting cellular individuality, tissue mosaicism**,** and developmental plasticity.

Many of the genes that reside within I/SCs are regulated by allelic exclusion. Allelic exclusion is a regulatory mechanism by which only one allele of a gene is expressed while the other is actively silenced, ensuring monoallelic expression in each cell. This process is well characterized in the immune system, where it plays a critical

role in B-cell and T-cell receptor gene rearrangements, ensuring that each lymphocyte produces a single antigen receptor [18]. Furthermore, functional monoallelic expression is achieved via a secondary mechanism that involves product inhibition. For example, in developing B cells, expression of a productive immunoglobulin heavy chain allele suppresses rearrangement and expression of the second allele, maintaining clonal specificity [18]. Allelic exclusion has also been observed in olfactory receptors, where product feedback ensures expression of a single allele of only one member of a large gene family, ensuring that each olfactory receptor neuron responds to a single odorant [2,33,57-60].

I/SC regulation acts through mechanisms distinct from X inactivation.

Numerous studies in both human and mouse cells support the notion that allele-specific epigenetic regulation of autosomal protein-coding genes is widespread [4,11,13,37,38,40,57,61,62]. Although stochastic monoallelic expression on autosomes may appear similar to X chromosome inactivation (XCI), the mechanisms behind them are distinct: First, XCI is initiated in preimplantation embryos, as early as the 4-8 cell stage in the mouse and 8-16 cell stage in humans [63-67], and later becomes established during differentiation of the inner cell mass of the blastocyst in both species [67,68]. In contrast, autosomal stochastic monoallelic expression appears later in development, with allelic biases that can be erased and reestablished during differentiation [10,38]. For example, a recent study found that allele-specific autosomal inactivation is absent during early blood lineage specification but detectable in hematopoietic stem cells and their differentiated progeny [9]. Second, in XCI, there is strong coordination along the chromosomes: genes on the active X chromosome share both expression and early replication profiles, whereas genes on the inactive X show silencing and late replication.

In contrast, autosomal inactivation lacks such coordination: allelic expression and replication timing are unlinked within a chromosome and independent across the genome [1,7,69]. Taken together, these observations indicate that autosomal allelic inactivation operates via a mechanism distinct from XCI [1,9].

An alternative model for haploinsufficiency

The relationship between genotype and phenotype is fundamental to understanding human genetic disease. At the scale of the whole genome, loss of function alleles are generally not deleterious when heterozygous and are therefore haplosufficient [21,24]. Not surprisingly, most of the loss of function mutations in single genes in humans are recessive [21,29]. Therefore, for most human disease genes a single normal allele is sufficient to achieve the typical phenotype. Dominantly inherited disorders comprise a diverse group of conditions that are often severe and poorly understood, except in cases of gain-of-function mutations, where dominant negative or interfering activities induce the abnormal phenotype. In addition, many dominantly inherited diseases result from copy number changes, either gain or loss of wild-type alleles [29,70]. Haploinsufficiency, predicted to apply to as much as 40% of the human genome [19,20], refers to a heterozygous deletion or complete loss-of-function mutation that results in an altered phenotype, indicating that a single normal allele is insufficient. The underlying molecular mechanisms responsible for most haploinsufficient human disease genes remain largely unknown.

The existence of two distinct populations of cells in XX individuals, one expressing genes from the maternally derived X chromosome and the other from the paternally derived X, has profound implications for both development and

the manifestation of X-linked diseases, where both dominant and recessive inheritance patterns are observed in females [29]. A key factor influencing these inheritance patterns is the presence or absence of cellular selection during development. In certain X-linked disorders, strong selection favors the survival or expansion of cells in which the mutant allele is on the inactive X chromosome, resulting in a predominance of wild-type cells and a clinical presentation consistent with X-linked recessive inheritance [21,26]. In contrast, when cellular selection is absent, heterozygous females typically retain a ~50:50 mosaic of wild-type and mutant-expressing cells. The presence of mutant-expressing cells, essentially null cells, is thought to underlie X-linked dominant phenotypes [27,71]. In such cases, heterozygous loss of function mutations leads to a condition of haploinsufficiency, in which the presence of a single normal allele is insufficient to maintain normal function. Interestingly, although single X-linked alleles are sufficient in males, the mosaic expression pattern in females unmasks phenotypic consequences that are otherwise hidden. This highlights an underappreciated mechanism of haploinsufficiency: the cellular mosaicism inherent to X inactivation can reduce effective gene dosage below functional thresholds in individuals with heterozygous mutations, particularly in tissues where cells expressing the mutant (null) allele persist.

One of the most striking implications of I/SC regulation is its relevance to human genetic disease, particularly those involving haploinsufficiency. Among the 979 genes mapped within human VERT regions, 272 are associated with monogenic diseases, including 87 with autosomal dominant inheritance, many of which are classified as haploinsufficient [29]. Our findings offer a new mechanistic model for autosomal haploinsufficiency: in the absence of compensatory upregulation

and/or cellular selection mechanisms, stochastic allelic inactivation results in or expands a functionally null cell population, even when one allele is wild type. This mirrors the situation observed in X-linked dominant disorders with loss of function mutations, where the absence of cellular selection results in the persistence of null cells. This model expands upon prior theories of haploinsufficiency that assume strict biallelic expression, which attribute dominant phenotypes to factors such as threshold-dependent expression, stoichiometric imbalance in multiprotein complexes, or inability to buffer expression noise [22-25]. In addition, our model fits nicely with a previous study that modeled stochastic gene expression of disease genes and proposed "haploinsufficiency syndromes might result from an increased susceptibility to stochastic delays of gene initiation or interruptions of gene expression" [72]. Our data suggest that epigenetically regulated stochastic AEI can contribute to pathogenic phenotypes in heterozygous individuals by either reducing the number of functional cells below a critical disease threshold or by disrupting the normal mosaicism of gene expression within disease-relevant tissues. This expands the conceptual framework of haploinsufficiency to include epigenetic, rather than purely genetic, sources of dosage reduction.

Limitations of our study.

While our findings provide substantial evidence for the existence and functional relevance of I/SCs, several important limitations remain to be addressed. First, the number of clones analyzed in our studies, while sufficient to identify robust patterns of AEI and VERT, limits our ability to fully capture the full spectrum of stochastic epigenetic states across the genome. For example, we frequently observe AEI of genes located adjacent to VERT regions, indicating that the boundaries of the epigenetic mechanisms functioning at I/SCs remain undefined. This raises important questions

about how far the influence of I/SC-associated regulation extends beyond the VERT region. In addition, the specific epigenetic marks, including DNA methylation, histone modifications, and chromatin accessibility, at key regulatory elements such as replication origins, enhancers, and promoters within I/SCs have yet to be mapped. Furthermore, the higher-order chromatin organization of I/SCs, including their relationship to topologically associating domains (TADs) and A/B compartments [49,73], remains largely unexplored and may hold critical insights into their regulatory architecture and functional constraints. Second, our analysis was conducted in a restricted number of cell types, namely LCLs and ACPs, and therefore does not represent the full diversity of I/SC usage across human tissues. Third, our study was limited to a small number of individuals, which may constrain the identification of inter-individual variability in I/SC regulation. Fourth, the developmental timing of I/SC establishment remains unresolved; it is unclear when during lineage commitment or differentiation these regions acquire their allele-specific states. A related and equally important question is whether I/SCs can be reset during reprogramming into induced pluripotent stem cells (iPSCs) and subsequently reestablished upon differentiation. This issue is particularly relevant given the widespread use of iPSCs in human disease modeling and regenerative medicine [74-76]. Understanding how I/SCs behave during cellular reprogramming and lineage specification will be critical for interpreting AEI-related phenotypes in iPSC-derived systems.

An additional open question is how the magnitude of stochastic AEI influences disease states, particularly in the context of variable penetrance and expressivity. For example, a recent study employed allelic expression ratios to identify functionally relevant AEI in genes associated with inborn errors of immunity, showing that individuals with the same pathogenic mutation can

exhibit divergent clinical outcomes depending on the degree of allelic imbalance [28]. These findings suggest that AEI can modulate disease severity, acting as an epigenetic layer of regulation that determines whether a given mutation manifests clinically. We anticipate that the biological significance of AEI will vary depending on the function of the gene, its dosage sensitivity, and the cellular context in which it is expressed. Addressing these questions will be essential for achieving a comprehensive understanding of the formation, function, and disease relevance of I/SCs in human biology.

Conclusion

In conclusion, our work extends the catalog of I/SCs in the human genome and supports a model in which stochastic, allele-specific epigenetic regulation at autosomal loci contributes to cellular diversity and disease susceptibility. Moreover, by identifying syntenic I/SCs in the mouse genome, our findings greatly enhance the potential utility of mouse models for mechanistic studies of disease-causing mutations at conserved loci. Our findings present a potential mechanism for incomplete penetrance, variable expressivity, and tissue-specific vulnerability, particularly in disorders caused by haploinsufficiency. In such cases, stochastic silencing of the wild-type allele in a subset of cells may lead to functional null states, even in heterozygous individuals, reducing the effective number of functional cells below a critical threshold. This may be especially relevant in the nervous system, where precise gene dosage is often essential for maintaining neuronal function. Moreover, I/SC regulation at disease genes raises the possibility that stochastic epigenetic regulation could act as an epigenetic modifier of disease risk, helping to explain why some individuals carrying pathogenic mutations remain asymptomatic. Understanding the full scope of I/SC

regulation in both normal development and disease pathogenesis will be essential for identifying novel regulatory mechanisms and potential therapeutic targets. As tools for single-cell and allele-resolved epigenomics continue to advance, I/SCs may emerge as key elements in both basic biology and precision medicine.

RESOURCE AVAILABILITY

Further information and requests for resources and reagents should be directed to and will be fulfilled by the lead contact, Mathew Thayer (thayerm@ohsu.edu)

Materials availability statement

All data generated or analyzed during this study are included in the manuscript and supporting files.

Acknowledgments:

M.J.T. was supported by NIH (R01GM130703, and RF1NS142814).
M.B.H was supported by NIH NCI 4K00CA245677-03
DMG was supported by NIH R01GM083337

Author Contribution Statement

MBH, MJT, and DMG conceived of the experimental design for the RNA expression and replication timing assays. KF performed the surgeries to obtain the amputed digits. BJ and PAY performed the ACP cultures and clone generation. MBH and AEV carried out the RNA-seq assays, including data analysis. MBH and AEV carried out the Repli-seq assays, including data analysis. PFC and PTS provided advice during preparation of the manuscript. MBH, DMG and MJT wrote the manuscript.

Declaration of interests

The authors declare no competing interests.

Literature Cited:

1. Heskett, M.B., Vouzas, A.E., Smith, L.G., Yates, P.A., Boniface, C., Bouhassira, E.E., Spellman, P.T., Gilbert, D.M., and Thayer, M.J. (2022). Epigenetic control of chromosome-associated lncRNA genes essential for replication and stability. Nature communications *13*, 6301. 10.1038/s41467-022-34099-7.
2. Goldmit, M., and Bergman, Y. (2004). Monoallelic gene expression: a repertoire of recurrent themes. Immunol Rev *200*, 197-214.
3. Chess, A., Simon, I., Cedar, H., and Axel, R. (1994). Allelic inactivation regulates olfactory receptor gene expression. Cell *78*, 823-834. 10.1016/s0092-8674(94)90562-2.
4. Chess, A. (2016). Monoallelic Gene Expression in Mammals. Annu Rev Genet *50*, 317-327. 10.1146/annurev-genet-120215-035120.
5. Stoffregen, E.P., Donley, N., Stauffer, D., Smith, L., and Thayer, M.J. (2011). An autosomal locus that controls chromosome-wide replication timing and mono-allelic expression. Hum Mol Genet *20*, 2366-2378.
6. Thayer, M.J. (2012). Mammalian chromosomes contain cis-acting elements that control replication timing, mitotic condensation, and stability of entire chromosomes. Bioessays *34*, 760-770.
7. Donley, N., Smith, L., and Thayer, M.J. (2015). ASAR15, A cis-Acting Locus that Controls Chromosome-Wide Replication Timing and Stability of Human Chromosome 15. PLoS Genet *11*, e1004923. 10.1371/journal.pgen.1004923.
8. Crowley, J.J., Zhabotynsky, V., Sun, W., Huang, S., Pakatci, I.K., Kim, Y., Wang, J.R., Morgan, A.P., Calaway, J.D., Aylor, D.L., et al. (2015). Analyses of allele-specific gene expression in highly divergent mouse crosses identifies pervasive allelic imbalance. Nat Genet *47*, 353-360. 10.1038/ng.3222.
9. Kubasova, N., Alves-Pereira, C.F., Gupta, S., Vinogradova, S., Gimelbrant, A., and Barreto, V.M. (2022). In Vivo Clonal Analysis Reveals Random Monoallelic Expression in Lymphocytes That Traces Back to Hematopoietic Stem Cells. Frontiers in cell and developmental biology *10*. 10.3389/fcell.2022.827774.
10. Marion-Poll, L., Forêt, B., Zielinski, D., Massip, F., Attia, M., Carter, A.C., Syx, L., Chang, H.Y., Gendrel, A.V., and Heard, E. (2021). Locus specific epigenetic modalities of random allelic expression imbalance. Nature communications *12*, 5330. 10.1038/s41467-021-25630-3.
11. Zwemer, L.M., Zak, A., Thompson, B.R., Kirby, A., Daly, M.J., Chess, A., and Gimelbrant, A.A. (2012). Autosomal monoallelic expression in the mouse. Genome Biol *13*, R10. 10.1186/gb-2012-13-2-r10.
12. Yagi, T. (2013). Genetic basis of neuronal individuality in the mammalian brain. Journal of neurogenetics *27*, 97-105. 10.3109/01677063.2013.801969.
13. Savova, V., Chun, S., Sohail, M., McCole, R.B., Witwicki, R., Gai, L., Lenz, T.L., Wu, C.T., Sunyaev, S.R., and Gimelbrant, A.A. (2016). Genes with monoallelic expression contribute disproportionately to genetic diversity in humans. Nat Genet *48*, 231-237. 10.1038/ng.3493.
14. Savova, V., Vigneau, S., and Gimelbrant, A.A. (2013). Autosomal monoallelic expression: genetics of epigenetic diversity? Curr Opin Genet Dev *23*, 642-648. 10.1016/j.gde.2013.09.001.
15. Johnstone, B., Stoddart, M.J., and Im, G.I. (2020). Multi-Disciplinary Approaches for Cell-Based Cartilage Regeneration. J Orthop Res *38*, 463-472. 10.1002/jor.24458.

16. Pattappa, G., Reischl, F., Jahns, J., Schewior, R., Lang, S., Zellner, J., Johnstone, B., Docheva, D., and Angele, P. (2021). Fibronectin Adherent Cell Populations Derived From Avascular and Vascular Regions of the Meniscus Have Enhanced Clonogenicity and Differentiation Potential Under Physioxia. Front Bioeng Biotechnol *9*, 789621. 10.3389/fbioe.2021.789621.
17. Rodriguez, I., Feinstein, P., and Mombaerts, P. (1999). Variable patterns of axonal projections of sensory neurons in the mouse vomeronasal system. Cell *97*, 199-208. 10.1016/s0092-8674(00)80730-8.
18. Mostoslavsky, R., Singh, N., Tenzen, T., Goldmit, M., Gabay, C., Elizur, S., Qi, P., Reubinoff, B.E., Chess, A., Cedar, H., and Bergman, Y. (2001). Asynchronous replication and allelic exclusion in the immune system. Nature *414*, 221-225.
19. Backman, J.D., Li, A.H., Marcketta, A., Sun, D., Mbatchou, J., Kessler, M.D., Benner, C., Liu, D., Locke, A.E., Balasubramanian, S., et al. (2021). Exome sequencing and analysis of 454,787 UK Biobank participants. Nature *599*, 628-634. 10.1038/s41586-021-04103-z.
20. Jurgens, S.J., Wang, X., Choi, S.H., Weng, L.C., Koyama, S., Pirruccello, J.P., Nguyen, T., Smadbeck, P., Jang, D., Chaffin, M., et al. (2024). Rare coding variant analysis for human diseases across biobanks and ancestries. Nat Genet *56*, 1811-1820. 10.1038/s41588-024-01894-5.
21. Zschocke, J., Byers, P.H., and Wilkie, A.O.M. (2023). Mendelian inheritance revisited: dominance and recessiveness in medical genetics. Nat Rev Genet *24*, 442-463. 10.1038/s41576-023-00574-0.
22. Huang, N., Lee, I., Marcotte, E.M., and Hurles, M.E. (2010). Characterising and predicting haploinsufficiency in the human genome. PLoS Genet *6*, e1001154. 10.1371/journal.pgen.1001154.
23. Morrill, S.A., and Amon, A. (2019). Why haploinsufficiency persists. Proc Natl Acad Sci U S A *116*, 11866-11871. 10.1073/pnas.1900437116.
24. Wilkie, A.O. (1994). The molecular basis of genetic dominance. J Med Genet *31*, 89-98. 10.1136/jmg.31.2.89.
25. Veitia, R.A., Zschocke, J., and Birchler, J.A. (2025). Gene Dosage Sensitivity and Human Genetic Diseases. J Inherit Metab Dis *48*, e70058. 10.1002/jimd.70058.
26. Minks, J., Robinson, W.P., and Brown, C.J. (2008). A skewed view of X chromosome inactivation. J Clin Invest *118*, 20-23. 10.1172/jci34470.
27. Boone, P.M., Buenaventura, T., King, J.W.D., and Merkenschlager, M. (2025). X-linked competition - implications for human development and disease. Nat Rev Genet. 10.1038/s41576-025-00840-3.
28. Stewart, O., Gruber, C., Randolph, H.E., Patel, R., Ramba, M., Calzoni, E., Huang, L.H., Levy, J., Buta, S., Lee, A., et al. (2025). Monoallelic expression can govern penetrance of inborn errors of immunity. Nature *637*, 1186-1197. 10.1038/s41586-024-08346-4.
29. McKusick, V. (2025). Online Mendelian Inheritance in Man, OMIM®.
30. Gilad, Y., Rifkin, S.A., and Pritchard, J.K. (2008). Revealing the architecture of gene regulation: the promise of eQTL studies. Trends Genet *24*, 408-415. 10.1016/j.tig.2008.06.001.
31. Heskett, M.B., Smith, L.G., Spellman, P., and Thayer, M.J. (2020). Reciprocal monoallelic expression of ASAR lncRNA genes controls replication timing of human chromosome 6. RNA (New York, N.Y.) *26*, 724-738. 10.1261/rna.073114.119.

32. Fu, R., Qin, P., Zou, X., Hu, Z., Hong, N., Wang, Y., and Jin, W. (2021). A Comprehensive Characterization of Monoallelic Expression During Hematopoiesis and Leukemogenesis via Single-Cell RNA-Sequencing. Frontiers in cell and developmental biology *9*, 702897. 10.3389/fcell.2021.702897.
33. Zakharova, I.S., Shevchenko, A.I., and Zakian, S.M. (2009). Monoallelic gene expression in mammals. Chromosoma *118*, 279-290.
34. Xu, J., Carter, A.C., Gendrel, A.V., Attia, M., Loftus, J., Greenleaf, W.J., Tibshirani, R., Heard, E., and Chang, H.Y. (2017). Landscape of monoallelic DNA accessibility in mouse embryonic stem cells and neural progenitor cells. Nat Genet *49*, 377-386. 10.1038/ng.3769.
35. Nag, A., Savova, V., Fung, H.L., Miron, A., Yuan, G.C., Zhang, K., and Gimelbrant, A.A. (2013). Chromatin signature of widespread monoallelic expression. eLife *2*, e01256. 10.7554/eLife.01256.
36. Li, S.M., Valo, Z., Wang, J., Gao, H., Bowers, C.W., and Singer-Sam, J. (2012). Transcriptome-wide survey of mouse CNS-derived cells reveals monoallelic expression within novel gene families. PLoS One *7*, e31751.
37. Gendrel, A.V., Marion-Poll, L., Katoh, K., and Heard, E. (2016). Random monoallelic expression of genes on autosomes: Parallels with X-chromosome inactivation. Semin Cell Dev Biol. 10.1016/j.semcdb.2016.04.007.
38. Gendrel, A.V., Attia, M., Chen, C.J., Diabangouaya, P., Servant, N., Barillot, E., and Heard, E. (2014). Developmental dynamics and disease potential of random monoallelic gene expression. Dev Cell *28*, 366-380. 10.1016/j.devcel.2014.01.016.
39. Eckersley-Maslin, M.A., Thybert, D., Bergmann, J.H., Marioni, J.C., Flicek, P., and Spector, D.L. (2014). Random monoallelic gene expression increases upon embryonic stem cell differentiation. Dev Cell *28*, 351-365. 10.1016/j.devcel.2014.01.017.
40. Barreto, V.M., Kubasova, N., Alves-Pereira, C.F., and Gendrel, A.V. (2021). X-Chromosome Inactivation and Autosomal Random Monoallelic Expression as "Faux Amis". Frontiers in cell and developmental biology *9*, 740937. 10.3389/fcell.2021.740937.
41. Blumenfeld, B., Masika, H., Farago, M., Yehuda, Y., Halaseh, L., Vardi, O., Rapoport, R., Levin-Klein, R., Cedar, H., Bergman, Y., and Simon, I. (2021). Chromosomal coordination and differential structure of asynchronous replicating regions. Nature communications *12*, 1035. 10.1038/s41467-021-21348-4.
42. Mountoufaris, G., Chen, W.V., Hirabayashi, Y., O'Keeffe, S., Chevee, M., Nwakeze, C.L., Polleux, F., and Maniatis, T. (2017). Multicluster Pcdh diversity is required for mouse olfactory neural circuit assembly. Science *356*, 411-414. 10.1126/science.aai8801.
43. Williams, D.L., Sikora, V.M., Hammer, M.A., Amin, S., Brinjikji, T., Brumley, E.K., Burrows, C.J., Carrillo, P.M., Cromer, K., Edwards, S.J., et al. (2021). May the Odds Be Ever in Your Favor: Non-deterministic Mechanisms Diversifying Cell Surface Molecule Expression. Frontiers in cell and developmental biology *9*, 720798. 10.3389/fcell.2021.720798.
44. Savova, V., Vinogradova, S., Pruss, D., Gimelbrant, A.A., and Weiss, L.A. (2017). Risk alleles of genes with monoallelic expression are enriched in gain-of-function variants and depleted in loss-of-function variants for neurodevelopmental disorders. Mol Psychiatry *22*, 1785-1794. 10.1038/mp.2017.13.

45. Gimelbrant, A., Hutchinson, J.N., Thompson, B.R., and Chess, A. (2007). Widespread monoallelic expression on human autosomes. Science *318*, 1136-1140.
46. Ito, H., Morishita, R., and Nagata, K.I. (2017). Autism spectrum disorder-associated genes and the development of dentate granule cells. Med Mol Morphol *50*, 123-129. 10.1007/s00795-017-0161-z.
47. Lin, L., Lesnick, T.G., Maraganore, D.M., and Isacson, O. (2009). Axon guidance and synaptic maintenance: preclinical markers for neurodegenerative disease and therapeutics. Trends Neurosci *32*, 142-149. 10.1016/j.tins.2008.11.006.
48. Mosca-Boidron, A.L., Gueneau, L., Huguet, G., Goldenberg, A., Henry, C., Gigot, N., Pallesi-Pocachard, E., Falace, A., Duplomb, L., Thevenon, J., et al. (2016). A de novo microdeletion of SEMA5A in a boy with autism spectrum disorder and intellectual disability. European journal of human genetics : EJHG *24*, 838-843. 10.1038/ejhg.2015.211.
49. Richer, S., Tian, Y., Schoenfelder, S., Hurst, L., Murrell, A., and Pisignano, G. (2023). Widespread allele-specific topological domains in the human genome are not confined to imprinted gene clusters. Genome Biol *24*, 40. 10.1186/s13059-023-02876-2.
50. Reutlinger, C., Helbig, I., Gawelczyk, B., Subero, J.I., Tönnies, H., Muhle, H., Finsterwalder, K., Vermeer, S., Pfundt, R., Sperner, J., et al. (2010). Deletions in 16p13 including GRIN2A in patients with intellectual disability, various dysmorphic features, and seizure disorders of the rolandic region. Epilepsia *51*, 1870-1873. 10.1111/j.1528-1167.2010.02555.x.
51. Ding, J., Li, X., Tian, H., Wang, L., Guo, B., Wang, Y., Li, W., Wang, F., and Sun, T. (2021). SCN1A Mutation-Beyond Dravet Syndrome: A Systematic Review and Narrative Synthesis. Front Neurol *12*, 743726. 10.3389/fneur.2021.743726.
52. Wolff, M., Johannesen, K.M., Hedrich, U.B.S., Masnada, S., Rubboli, G., Gardella, E., Lesca, G., Ville, D., Milh, M., Villard, L., et al. (2017). Genetic and phenotypic heterogeneity suggest therapeutic implications in SCN2A-related disorders. Brain *140*, 1316-1336. 10.1093/brain/awx054.
53. Hernandez, C.C., Hu, N., Shen, W., and Macdonald, R.L. (2023). Epileptic Encephalopathy GABRB Structural Variants Share Common Gating and Trafficking Defects. Biomolecules *13*. 10.3390/biom13121790.
54. Hamdan, F.F., Myers, C.T., Cossette, P., Lemay, P., Spiegelman, D., Laporte, A.D., Nassif, C., Diallo, O., Monlong, J., Cadieux-Dion, M., et al. (2017). High Rate of Recurrent De Novo Mutations in Developmental and Epileptic Encephalopathies. Am J Hum Genet *101*, 664-685. 10.1016/j.ajhg.2017.09.008.
55. Gruber, C.N., Calis, J.J.A., Buta, S., Evrony, G., Martin, J.C., Uhl, S.A., Caron, R., Jarchin, L., Dunkin, D., Phelps, R., et al. (2020). Complex Autoinflammatory Syndrome Unveils Fundamental Principles of JAK1 Kinase Transcriptional and Biochemical Function. Immunity *53*, 672-684.e611. 10.1016/j.immuni.2020.07.006.
56. Ross, S.H., and Cantrell, D.A. (2020). Of Mosaicism and Mechanisms: How JAK1 Goes Awry. Immunity *53*, 481-484. 10.1016/j.immuni.2020.08.010.
57. Khamlichi, A.A., and Feil, R. (2018). Parallels between Mammalian Mechanisms of Monoallelic Gene Expression. Trends Genet *34*, 954-971. 10.1016/j.tig.2018.08.005.

58. Dalton, R.P., Lyons, D.B., and Lomvardas, S. (2013). Co-opting the unfolded protein response to elicit olfactory receptor feedback. Cell *155*, 321-332. 10.1016/j.cell.2013.09.033.
59. Lyons, D.B., Allen, W.E., Goh, T., Tsai, L., Barnea, G., and Lomvardas, S. (2013). An epigenetic trap stabilizes singular olfactory receptor expression. Cell *154*, 325-336. 10.1016/j.cell.2013.06.039.
60. Pourmorady, A.D., Bashkirova, E.V., Chiariello, A.M., Belagzhal, H., Kodra, A., Duffié, R., Kahiapo, J., Monahan, K., Pulupa, J., Schieren, I., et al. (2024). RNA-mediated symmetry breaking enables singular olfactory receptor choice. Nature *625*, 181-188. 10.1038/s41586-023-06845-4.
61. Chess, A. (2012). Mechanisms and consequences of widespread random monoallelic expression. Nat Rev Genet *13*, 421-428.
62. Reinius, B., and Sandberg, R. (2015). Random monoallelic expression of autosomal genes: stochastic transcription and allele-level regulation. Nat Rev Genet *16*, 653-664. 10.1038/nrg3888.
63. Brockdorff, N., and Turner, B.M. (2015). Dosage compensation in mammals. Cold Spring Harb Perspect Biol *7*, a019406. 10.1101/cshperspect.a019406.
64. Dossin, F., and Heard, E. (2022). The Molecular and Nuclear Dynamics of X-Chromosome Inactivation. Cold Spring Harb Perspect Biol *14*. 10.1101/cshperspect.a040196.
65. Galupa, R., and Heard, E. (2018). X-Chromosome Inactivation: A Crossroads Between Chromosome Architecture and Gene Regulation. Annu Rev Genet *52*, 535-566. 10.1146/annurev-genet-120116-024611.
66. Payer, B., and Lee, J.T. (2008). X chromosome dosage compensation: how mammals keep the balance. Annu Rev Genet *42*, 733-772. 10.1146/annurev.genet.42.110807.091711 [doi].
67. van den Berg, I.M., Galjaard, R.J., Laven, J.S., and van Doorninck, J.H. (2011). XCI in preimplantation mouse and human embryos: first there is remodelling…. Hum Genet *130*, 203-215. 10.1007/s00439-011-1014-9.
68. van den Berg, I.M., Laven, J.S., Stevens, M., Jonkers, I., Galjaard, R.J., Gribnau, J., and van Doorninck, J.H. (2009). X chromosome inactivation is initiated in human preimplantation embryos. Am J Hum Genet *84*, 771-779. 10.1016/j.ajhg.2009.05.003.
69. Donley, N., Stoffregen, E.P., Smith, L., Montagna, C., and Thayer, M.J. (2013). Asynchronous Replication, Mono-Allelic Expression, and Long Range Cis-Effects of ASAR6. PLoS Genet *9*, e1003423.
70. Rehm, H.L., Berg, J.S., Brooks, L.D., Bustamante, C.D., Evans, J.P., Landrum, M.J., Ledbetter, D.H., Maglott, D.R., Martin, C.L., Nussbaum, R.L., et al. (2015). ClinGen--the Clinical Genome Resource. N Engl J Med *372*, 2235-2242. 10.1056/NEJMsr1406261.
71. Giovenino, C., Trajkova, S., Pavinato, L., Cardaropoli, S., Pullano, V., Ferrero, E., Sukarova-Angelovska, E., Carestiato, S., Salmin, P., Rinninella, A., et al. (2023). Skewed X-chromosome inactivation in unsolved neurodevelopmental disease cases can guide re-evaluation For X-linked genes. European journal of human genetics : EJHG *31*, 1228-1236. 10.1038/s41431-023-01324-w.
72. Cook, D.L., Gerber, A.N., and Tapscott, S.J. (1998). Modeling stochastic gene expression: implications for haploinsufficiency. Proc Natl Acad Sci U S A *95*, 15641-15646. 10.1073/pnas.95.26.15641.

73. Pope, B.D., Ryba, T., Dileep, V., Yue, F., Wu, W., Denas, O., Vera, D.L., Wang, Y., Hansen, R.S., Canfield, T.K., et al. (2014). Topologically associating domains are stable units of replication-timing regulation. Nature *515*, 402-405. 10.1038/nature13986.
74. Li, Y., and Darabi, R. (2022). Role of epigenetics in cellular reprogramming; from iPSCs to disease modeling and cell therapy. J Cell Biochem *123*, 147-154. 10.1002/jcb.30164.
75. Janiszewski, A., Talon, I., Chappell, J., Collombet, S., Song, J., De Geest, N., To, S.K., Bervoets, G., Marin-Bejar, O., Provenzano, C., et al. (2019). Dynamic reversal of random X-Chromosome inactivation during iPSC reprogramming. Genome Res *29*, 1659-1672. 10.1101/gr.249706.119.
76. Tcw, J. (2019). Human iPSC application in Alzheimer's disease and Tau-related neurodegenerative diseases. Neurosci Lett *699*, 31-40. 10.1016/j.neulet.2019.01.043.
77. Pattappa, G., Markway, B.D., Docheva, D., and Johnstone, B. (2023). Physioxic Culture of Chondrogenic Cells. Methods Mol Biol *2598*, 45-63. 10.1007/978-1-0716-2839-3_5.
78. Li, H., and Durbin, R. (2009). Fast and accurate short read alignment with Burrows-Wheeler transform. Bioinformatics (Oxford, England) *25*, 1754-1760. 10.1093/bioinformatics/btp324.
79. Garrison, E.a.M., G (2024). Haplotype-based variant detection from short-read sequencing. arXiv *1207.3907v2*.
80. Martin, M., Ebert, P., and Marschall, T. (2023). Read-Based Phasing and Analysis of Phased Variants with WhatsHap. Methods Mol Biol *2590*, 127-138. 10.1007/978-1-0716-2819-5_8.
81. Li, H., Handsaker, B., Wysoker, A., Fennell, T., Ruan, J., Homer, N., Marth, G., Abecasis, G., and Durbin, R. (2009). The Sequence Alignment/Map format and SAMtools. Bioinformatics (Oxford, England) *25*, 2078-2079. 10.1093/bioinformatics/btp352.
82. Marchal, C., Sasaki, T., Vera, D., Wilson, K., Sima, J., Rivera-Mulia, J.C., Trevilla-García, C., Nogues, C., Nafie, E., and Gilbert, D.M. (2018). Genome-wide analysis of replication timing by next-generation sequencing with E/L Repli-seq. Nat Protoc *13*, 819-839. 10.1038/nprot.2017.148.
83. Dobin, A., Davis, C.A., Schlesinger, F., Drenkow, J., Zaleski, C., Jha, S., Batut, P., Chaisson, M., and Gingeras, T.R. (2013). STAR: ultrafast universal RNA-seq aligner. Bioinformatics (Oxford, England) *29*, 15-21. 10.1093/bioinformatics/bts635.

Methods

Cell culture

All human tissue samples were obtained in accordance with protocols approved by the Oregon Health & Science University Institutional Review Board (OHSU IRB# 00019018) and the Western Institutional Review Board (WIRB# 20193303). Informed consent was obtained from all donors or their legal guardians. ACP cells were grown in Dulbecco's Modified Eagle's Medium low glucose (Life Technologies) supplemented with 10% fetal bovine serum (Hyclone). Single cell clones were isolated by plating individual cells in 6 well dishes, and were expanded for >20 population doublings [77]. All cells were grown in a humidified incubator at 37°C in a 5% carbon dioxide atmosphere.

Haplotype Phasing of ACP cells

Short-read whole genome sequencing was obtained from two parent/child trios with a range of ~7-14x genome coverage. BWA [78] was used for alignment, and FreeBayes [79] used to call putative germline variants jointly for each trio. Variants were filtered to remove sites with Genotype Quality score of less than 30, and sites with missing genotypes for any member of the trio were removed. WhatsHap [80] was then used to phase variants in the child utilizing mendelian inheritance patterns and reads containing multiple variants. 1,679,207 high-confidence sites were phased in ACP7, and 837,323 sites were phased in ACP6.

Allele-specific Repli-Seq

Short read sequence data was aligned with BWA with standard parameters. BAM files were then deduplicated and sorted with SAMtools [81]. BCFtools mpileup [81] was then used to produce allele-specific read counts at phased heterozygous loci. Library size

normalization was performed to produce counts per million informative reads. Read counts were then grouped into 250kb sliding genomic windows with no overlap. E/L Repli-Seq values were generated by taking the Log base 2 of early versus late values [82]. Quantile normalization was performed on each group of subclones within each individual sample to allow for comparison among subclones. For each sample, variability of allele-specific RT among subclones was defined as the Standard Deviation (degrees of freedom = 1) of repli-seq at each 250kb window. Genome-wide std. dev. values generated a log-normal distribution, and we set a threshold of Z>=2.25 on the log-normal to identify regions with highly variable allele-specific RT among subclones.

Allele-specific RNA-seq

Nuclei were isolated by centrifugation for 0.5 minutes from ACP clones following lysis in 0.5% NP40, 140 mM NaCl, 10 mM Tris-HCl (pH 7.4), and 1.5 mM $MgCl_2$. Nuclear RNA was isolated using Trizol reagent using the manufacturer's instructions, followed by DNase treatment to remove possible genomic DNA contamination. Briefly, ribosomal RNAs were removed using the Ribo-Zero kit (Illumina), RNA was fragmented into 250-300bp fragments, and cDNA libraries were prepared using the Directional RNA Library Prep Kit (NEB). Paired end sequencing was done on a NovaSeq 6000 at the OHSU MPSSR core facility. Strand specific short read sequence data was aligned with STAR [83]. SAMtools [81] was used to remove duplicates and sort BAM files. Strand-specific, allele-specific reads at heterozygous phased SNPs were counted using BCFtools mpileup [81] and grouped together for all SNPs within each gene. Allelic expression imbalance was calculated as the fraction of reads derived from the maternal vs the paternal allele. For example, completely balanced allelic expression is 50% AEI, and completely imbalanced AEI is 100%. A threshold of AEI>= 70%, and FDR corrected

binomial p-value<=0.05 was used to classify AEI in each individual subclone. Standard deviation (degrees of freedom=1) was used for each gene to generate a metric of AEI variability among subclones. A genome-wide distribution of std. dev. was generated across all genes, and the top 2.5% of variable genes were classified as highly variable among subclones.

Figure Legends:

Figure 1: Genome wide variable replication-timing and expression. a) Single cell derived ACP clones (color coded) are isolated, expanded and processed for Repliseq and RNAseq. The maternal and paternal haplotypes were used to analyze allele-specific replication timing and expression. b) The top panel illustrates the expected replication timing profile in multiple clones across an autosomal region. The regions that display VERT are highlighted by shading. The bottom panel illustrates the expected expression variability in different clones from the same individual. c) We define AEI as an allelic bias that is ≥80% allelic imbalance (AEI ≥ 0.80 or ≤ 0.20). d) Illustration of an Inactivation/Stability Center showing the clonal and allele-restricted variability in replication timing and expression of both protein coding and noncoding genes. e) The standard deviation (Std. Dev.) in 250 kb windows (circles) across human chromosome 1. Outlier windows from all four sets of clones (ACP6, ACP7, EB3-2, and GM12878) are highlighted in different colors as shown. The top panel illustrates the G-banding (blue shading) pattern for human chromosome 1, with 23 VERT regions highlighted in red. The arrow marks the VERT region shown in panels f-h below. f-h) I/SC located between 239 and 242 mb of chromosome 1 (see panel e). f) VERT (shaded region) and AEI of genes (rectangles) detected in the ACP6 clones, each clone was color coded as shown. For replication, the solid lines represent the maternal (Mat.) allele and the dotted line represents the paternal (Pat.) allele. g) VERT (shaded region) and AEI of genes (rectangles) detected in the ACP7 clones, each clone was color coded as shown. h) UCSC Genome Browser view of the genomic region in panels f and g. The shaded area highlights the VERT region. i) Hierarchical clustering of the VERT regions that are shared between 2 or more clone sets showing both ACP and LCL clones. j) Gene Ontology (GO) enrichment analysis of the genes located within the VERT regions, the most significant hits for each set of clones, organized by cell type, are shown. GO analysis of the mouse genes located within the pre-B cell clone VERT regions are also shown.

Figure 2. Examples of I/SCs. a, d and g) VERT regions on human chromosomes 18, 6 and 9, respectively. The top panels illustrate the G-banding (blue shading) pattern for each human chromosome, with VERT regions highlighted in red. The standard deviation (Std. Dev.) in 250 kb windows (circles) across each human chromosome is shown. Outlier windows from all four sets of clones (ACP6, ACP7, EB3-2, and GM12878) are highlighted in different colors as shown. The arrows and red boxes mark the VERT regions shown in panels b, e, and h. b, e and h) I/SCs highlighted in panels a, d, and g. For replication, the solid lines represent the maternal (Mat.) allele and the dotted line represents the paternal (Pat.) allele. The regions with VERT are shaded and the AEI is shown for each clone in a different color. c, f and i) UCSC Genome Browser views of the genomic regions in panels b, e and h. The shaded areas highlight the VERT regions. Genes with AEI are marked with +, *, or #. b and c) The + marks MOCOS, which shows AEI in ACP cells (Supplemental Table 2) and ++ marks FHOD3, which shows AEI in LCLs [1]. e and f) The * marks from DNAH8, ** marks transcripts from KCNK5, and *** marks non-coding transcripts from ENSG00000293066 (also named: TL:6-39.9_1 [1]). All three of these genes show AEI in LCL clones [1]. h and i) The # marks

transcripts from DAPK1, ## marks transcripts from SPIN1. Both genes show AEI in LCL clones [1].

Figure 3. Human gene clusters with AEI map to VERT regions. a and c) VERT regions on human chromosome 9 and 6. The top panels illustrate the G-banding (blue shading) pattern for each human chromosome, with VERT regions highlighted in red. The standard deviation (Std. Dev.) in 250 kb windows (circles) across each human chromosome is shown. Outlier windows from all four sets of clones (ACP6, ACP7, EB3-2, and GM12878) are highlighted in different colors as shown. The arrows and red boxes mark the VERT regions shown in panels b, e, and h. The red box and arrow identify the I/SC in panel b. b) UCSC genome browser view illustrating the genomic location highlighted in panel a. The shaded area highlights the VERT region. The red lines mark 11 olfactory receptor genes, and the green lines mark 6 cytochrome P450 family (CYP4F) genes. d) UCSC Genome Browser view illustrating the genomic location highlighted in panel c. The shaded area highlights the VERT region. The red lines mark 16 HLA genes, and the green lines mark 6 Lymphocyte antigen 6 family (LY6G) genes.

Figure 4. Mouse gene clusters with AEI map to VERT regions. a and d) VERT regions on mouse chromosome 2 and 18. The standard deviation (Std. Dev.) in 50 kb windows (circles) across each mouse chromosome are shown. Outlier windows from pre-B cell clones are highlighted in orange. The red boxes and arrows identify the VERT regions in panels b (i) and c (ii). b and c) UCSC genome browser views illustrating the genomic locations represented by i and ii in panel a. b) Genome Browser view of the VERT region showing the location of 29 olfactory receptor genes (Or genes). The shaded area represents the VERT region. c) Genome Browser view of the VERT region in ii above, showing the location of 242 olfactory receptor genes (Or genes). The shaded area represents the VERT region. e) Genome Browser view of the VERT region in d above, showing the location of clustered Protocaderhin genes (15 Pcdha, 23 Pcdhb, and 22 Pcdhg genes). The shaded area represents the VERT region.

Figure 5. Human and Mouse syntenic regions display VERT. a and b) The short arm of human chromosome 5, with 11 VERT regions (panel a) and the centromeric region of mouse chromosome 15, with 4 VERT regions (panel b) are shown. a) Two human VERT regions are highlighted, hi and hii, and are syntenic with locations on mouse chromosome 15, mi and mii, that also show VERT (panel b). Note that the gene order in both syntenic regions are inverted with respect to the telomeres when comparing the human and mouse loci. c) Illustration of the I/SC on human chromosome 5 between 7.75 and 10.5 mb (hi). The shaded area marks the VERT region, and AEI of the coding gene SEMA5A in different clones is highlighted. For replication, the maternal (Mat.) and paternal (Pat.) alleles are indicated. d) UCSC Genome Browser view of the human VERT region (shaded) in hi, showing the location of SEMA5A and a taste receptor gene (TAS2R1). e) UCSC Genome Browser view of the mouse VERT region (shaded) in mi, showing the location of Sema5a and a taste receptor gene (Tas2r119). f) UCSC Genome Browser view of the human VERT region (shaded) in hii above, highlighting the location of the AEI gene RETREG1 [45]. g) UCSC Genome Browser view of the mouse VERT region (shaded) in mii, showing the synteny between human and mouse for the protein coding genes in panel f, including Retreg1. h) VERT regions on human

chromosome 16. The standard deviation (Std. Dev.) in 250 kb windows (circles) across human chromosome 16 is shown. Outlier windows are highlighted in different colors as shown. The red box and arrow mark the genomic location in panel i. i) UCSC Genome Browser view illustrating the genomic location represented in panel h, showing the location of GRIN2A (red box). j) VERT regions on mouse chromosome 16. The standard deviation in 50 kb windows (circles) is shown. Outlier windows from pre-B cell clones are highlighted in orange. k) UCSC Genome Browser view illustrating the genomic location of the VERT region (shaded area) represented in panel j above, with the location of Grin2a highlighted with a red box.

Figure 6. Epilepsy genes map to I/SCs. a, d, and g) VERT regions on human chromosomes 2, 5, and 21. The top panels illustrate the G-banding (blue shading) pattern for each human chromosome, with VERT regions highlighted in red. The standard deviation (Std. Dev.) in 250 kb windows (circles) across each human chromosome is shown. Outlier windows from all four sets of clones (ACP6, ACP7, EB3-2, and GM12878) are highlighted in different colors as shown. The arrows and red boxes mark the VERT regions shown in panels b, c, e, f, h, i, j and k. b, e, h, j) Illustrations of I/SCs on chromosomes 2, 5, and 8. The shaded areas mark the VERT regions. Each clone was color coded to illustrate the VERT and AEI in different clones. The maternal (Mat.) and paternal (Pat.) alleles are indicated for replication and expression. c) UCSC Genome Browser view illustrating the genomic location of the VERT region (shaded area) represented in panels a and b, with the location of 5 sodium channel genes (SCN3A, SCN2A, SCN1A, SCN9A, and SCN7A) highlighted with a red line. e) Illustration of an I/SC on chromosome 5. The shaded area marks the VERT region. AEI of GABRA1 is shown. f) UCSC Genome Browser view illustrating the genomic location of the VERT region (shaded area) represented in panels d and e above, with the location of 4 GABA receptor genes (GABRB2, GABRBA6, GABRA1, and GABRG2) highlighted with a red line. h) Illustration of a I/SCs (A) on chromosome 8. Each ACP6 clone was color coded to illustrate the VERT and AEI in different clones. The maternal (Mat.) and paternal (Pat.) alleles are indicated for replication and expression. The shaded area marks the VERT region. The location and expression of OXR1 is indicated. i) UCSC Genome Browser view illustrating the genomic location of the VERT region (shaded area) represented in panels g (A) and h above, with the location of the OXR1 gene highlighted with a red line. We note that ANGPT1 (marked with *), located within this I/SC displays AEI (see Supplementary Table 2). j) Illustration of an I/SC (B) on chromosome 8. AEI of SAMD12 is indicated. k) UCSC Genome Browser view illustrating the genomic location of the VERT region (shaded area) represented in panels g (B) and j above, with the location of the SAMD12 highlighted with a red line.

Figure 7. Parkinson disease genes map to I/SCs. a, c, e, and g) VERT regions on human chromosomes 4, 12, 19, and 20, respectively. The top panels illustrate the G-banding (blue shading) pattern for each human chromosome, with VERT regions highlighted in red. The standard deviation (Std. Dev.) in 250 kb windows (circles) across each human chromosome is shown. Outlier windows from all four sets of clones (ACP6, ACP7, EB3-2, and GM12878) are highlighted in different colors as shown. The arrows and red boxes mark the VERT regions shown in panels b, d, f, and h, respectively. b) UCSC Genome Browser view illustrating the genomic location of the VERT region (shaded area) represented in panel a, with the location of the SNCA gene highlighted with a red line. d) UCSC Genome Browser view illustrating the genomic location of the VERT region (shaded

area) highlighted in panel c, with the location of the LRRK2 gene highlighted with a red line. f) UCSC Genome Browser view illustrating the genomic location of the VERT region (shaded area) represented in panel e, with the location of the DNAJC6 gene highlighted with a red line; also highlighted with a green line is the JAK1 gene. h) UCSC Genome Browser view illustrating the genomic location of the VERT region (shaded area) represented in panel g, with the location of the PRKN gene highlighted with a red line.

RESOURCE AVAILABILITY

Source data are provided with this paper. Further information and requests for resources and reagents should be directed to and will be fulfilled by the lead contact, Mathew Thayer (thayerm@ohsu.edu).

Materials availability statement

All reagents generated in this study will be made freely available upon request.

Human VERT Region			Gene Cluster			
Chr	Start	stop	Genes	# of Genes	Start	stop
1	13,250,000	15,000,000	PRAMEF	23	12,768,939	13,422,488
2	101,633,538	102,383,540	IL1R	5	101,987,899	102,401,443
2	165,250,000	166,000,000	SCN	5	165,081,204	166,499,088
2	176,250,000	176,500,000	HOXD	9	176,091,062	176,191,493
4	46,750,000	47,500,000	GABR	4	46,035,583	47,431,569
4	68,384,282	68,634,282	UGT	9	68,525,283	69,660,413
5	651,700	750,000	SLC	5	468,888	1,448,927
5	148,000,000	148,250,000	SPINK	7	147,822,992	148,343,066
5	162,250,000	162,750,000	GABR	4	161,282,809	162,159,566
6	31,250,000	32,750,000	HLA	15	30,489,509	33,093,613
			LY6	6	31,669,259	31,722,476
8	11,250,000	12,392,491	DEFB	6	11,970,747	12,320,078
8	80,587,765	83,000,000	FABP	4	81,277,942	81,536,065
8	142,500,000	142,750,000	LY6	8	142,695,707	143,162,219
11	104,750,000	105,000,000	CASP	5	104,883,181	105,141,441
15	23,357,400	23,500,000	GOLGA	5	22,451,995	23,451,545
15	28,750,000	29,000,000	GOLGA	6	28,344,604	28,855,059
17	9,750,000	10,500,000	MYH	6	10,297,552	10,658,865
19	15,000,000	15,250,000	OR	11	14,792,476	15,952,060
			CYP	6	15,507,105	15,936,041
19	20,750,000	21,000,000	ZNF	37	19,667,773	24,119,420
19	36,313,700	36,500,000	ZNF	29	36,171,632	37,791,237
19	43,000,000	43,250,000	PSG	10	42,713,521	43,272,861
20	24,250,000	24,750,000	CST	11	23,429,902	24,957,423
21	30,627,681	30,877,681	KRTAP	33	30,276,201	31,041,124

Mouse VERT Region			Gene Cluster			
Chr	Start	stop	Genes	# of Genes	Start	stop
2	36,322,857	36,622,857	Or	28	36,225,624	37,193,679
2	64,622,866	66,522,868	Scn	5	65,287,042	66,637,709
2	88,950,000	89,950,000	Or	239	85,160,859	90,147,389
4	59,850,000	59,950,000	Mup	22	59,950,000	61,824,646
5	91,150,000	91,350,000	Cxcl	5	91,186,938	91,335,955
5	95,950,000	96,250,000	Pramel	23	93,891,822	96,243,866
6	40,650,000	41,150,000	Tas2r	8	40,386,430	43,196,843
			Or	24	40,386,430	43,196,843
6	66,650,000	66,850,000	Vmn1	8	66,498,911	66,758,688
7	113,809,945	113,909,945	Or	24	113,790,926	114,306,041
11	73,450,000	74,050,000	Or	31	73,160,403	74,180,092
18	37,350,000	37,750,000	Pcdh	23	37,298,052	37,684,088

Table 1. VERT regions at gene clusters in the human and mouse genomes

Mouse VERT				Human Syntenic Region			Human VERT		
Chr	Start	stop	Synteny (%)	Chr	start	Stop	Chr	start	Stop
1	73,042,585	73,542,585	54.0	2	216,836,864	217,400,721	2	217,000,000	217,250,000
1	88,681,147	89,081,147	33.0	2	234,565,154	235,053,857	2	234,000,000	235,000,000
1	189558318	189,758,318	49.8	1	214,144,079	214,410,956	1	214,326,657	216,000,000
2	64,842,287	66,742,287	46.5	2	164,610,983	166,685,353	2	165,250,000	166,000,000
3	18,204,164	18,404,164	33.7	8	64,684,742	64,876,026	8	64,337,443	65,087,765
3	57,253,499	58,553,499	32.6	3	149,407,811	150,704,641	3	149,282,213	150,032,213
3	78,253,385	78,653,385	26.1	4	159,655,594	159,952,325	4	159,328,848	159,828,848
3	82,453,385	82,853,385	32.6	4	154,688,934	155,210,940	4	154,500,000	154,750,000
4	105034592	105,234,592	62.8	1	56,331,724	56,556,339	1	55,500,000	56,750,000
4	142286667	142,686,667	40.6	1	14,022,915	14,523,879	1	13,250,000	15,000,000
8	10,500,000	11,200,000	43.2	13	108,978,718	110,065,357	13	109,250,000	109,500,000
8	24,029,544	24,929,544	37.3	8	40,152,844	41,090,451	8	40,250,000	40,750,000
8	39,817,687	40,717,687	28.6	8	15,936,545	16,964,053	8	15,750,000	17,000,000
9	116969950	117,469,950	42.3	3	28,837,647	29,402,683	3	29,000,000	29,500,000
11	46,927,325	48,127,325	35.2	5	155,465,678	156,698,430	5	155,500,000	156,250,000
12	33,715,134	33,815,134	36.1	7	19,330,767	19,416,599	7	19,250,000	19,500,000
12	105278049	105,578,049	41.6	14	95,853,630	96,269,387	14	96,000,000	96,250,000
13	11,095,964	11,672,619	29.9	1	237,711,340	238,470,922	1	237,604,200	238,750,000
15	25,120,331	25,920,331	42.9	5	16,534,412	17,724,462	5	16,250,000	17,000,000
15	32,220,391	32,420,391	60.7	5	9,377,059	9,575,503	5	8,749,888	9,499,888
16	9,067,771	9,667,771	41.6	16	9,476,924	10,028,307	16	9,750,000	10,000,000

Table 2. VERT regions showing synteny between human and mouse genomes.

VERT Gene	Epilepsy Disease Genes (Inheritance: Autosomal Recessive-AR; Autosomal Dominant-AD; Loss of Function-LoF; Gain of Function-GoF)	Ref.
ALG14	Myasthenic syndrome (AR); Intellectual developmental disorder with epilepsy (AR); Myopathy, epilepsy, and progressive cerebral atrophy (AR)	29
CACNA2D1	Developmental and epileptic encephalopathy (AR)	29
GABRB1	Developmental and epileptic encephalopathy (AD, LoF & GoF)	53
GRIN2A	Epilepsy (AD, LoF)	50
NTRK2	Developmental and epileptic encephalopathy (AD); Obesity (AD)	54
OXR1	Cerebellar hypoplasia/atrophy, epilepsy, and global developmental delay (AR)	29
RAPGEF2	Epilepsy, familial adult myoclonic (AD, TTTCA repeat expansion)	55
RNF13	Developmental and epileptic encephalopathy (AD, GoF)	56
SAMD12	Epilepsy (AD, TTTCA repeat expansion)	55
SCN1A	Developmental and epileptic encephalopathy (AD, LoF); Dravet syndrome (AD, LoF); Generalized epilepsy with febrile seizures (AD, LoF)	51
SCN2A	Developmental and epileptic encephalopathy (AD, LoF & GoF)	52

VERT Gene	Intellectual Developmental Genes (Inheritance: Autosomal Recessive-AR; Autosomal Dominant-AD; Loss of Function-LoF; Gain of Function-GoF)	Ref.
ALG14	Intellectual developmental disorder with epilepsy (AR); Myasthenic syndrome (AR); Myopathy, epilepsy, and progressive cerebral atrophy (AR)	29
CEP104	Intellectual developmental disorder (AR); Joubert syndrome (AR)	29
CNOT2	Intellectual developmental disorder (AD, LoF)	53
DPP6	Intellectual developmental disorder (AD, LoF)	54
ELP2	Intellectual developmental disorder (AR)	29
FMN2	Intellectual developmental disorder (AR)	29
GRIA1	Intellectual developmental disorder (AD, GoF; AR, LoF)	55
IMPA1	Intellectual developmental disorder (AR)	29
IQSEC1	Intellectual developmental disorder (AR)	29
MYT1L	Intellectual developmental disorder (AD, LoF)	56
PDZD8	Intellectual developmental disorder (AR)	29
RSRC1	Intellectual developmental disorder (AR)	29
TAF4	Intellectual developmental disorder (AD, LoF)	57
TNIK	Intellectual developmental disorder (AR)	29
TUSC3	Intellectual developmental disorder (AR)	29
ZBTB18	Intellectual developmental disorder (AD, LoF)	58

VERT Gene	Neurodevelopment Disease Genes (Inheritance: Autosomal Recessive-AR; Autosomal Dominant-AD; Loss of Function-LoF; Gain of Function-GoF)	Ref.
ATP8A2	Cerebellar ataxia (AR)	29
CSNK2B	Poirier-Bienvenu neurodevelopmental syndrome (AD, LoF)	53
DPH5	Neurodevelopmental disorder (AR)	29
KCNA1	Episodic ataxia/myokymia syndrome (AD, LoF & GoF)	54,55
LMBRD2	Developmental delay with variable neurologic and brain abnormalities (AD)	29
NBEA	Neurodevelopmental disorder (AD, LoF)	56
RETREG1	Neuropathy (AR)	29
ROBO1	Nystagmus (AR); Neurooculorenal syndrome (AR); Pituitary hormone deficiency (AD)	29
TIAM1	Neurodevelopmental disorder (AR)	29
TRPM3	Neurodevelopmental disorder (AD, GoF)	57
VARS1	Neurodevelopmental disorder with microcephaly (AR)	29
ZSWIM6	Acromelic frontonasal dysostosis, (AD); Neurodevelopmental disorder (AD, GoF)	58,59

VERT Gene	Parkinson Disease Gene (Inheritance: Autosomal Recessive-AR; Autosomal Dominant-AD; Loss of Function-LoF; Gain of Function-GoF)	Ref.
DNAJC6	Parkinson disease 19 (AR)	29
LRRK2	Parkinson disease (AD, GoF)	60,61
PRKN	Parkinson disease (AR)	29
SLC18A2	Parkinsonism-dystonia (AR)	29
SNCA	Parkinson disease 1 & 4 (AD, LoF/GoF)	62-64

Table 3. Neurodevelopmental genes within VERT regions.

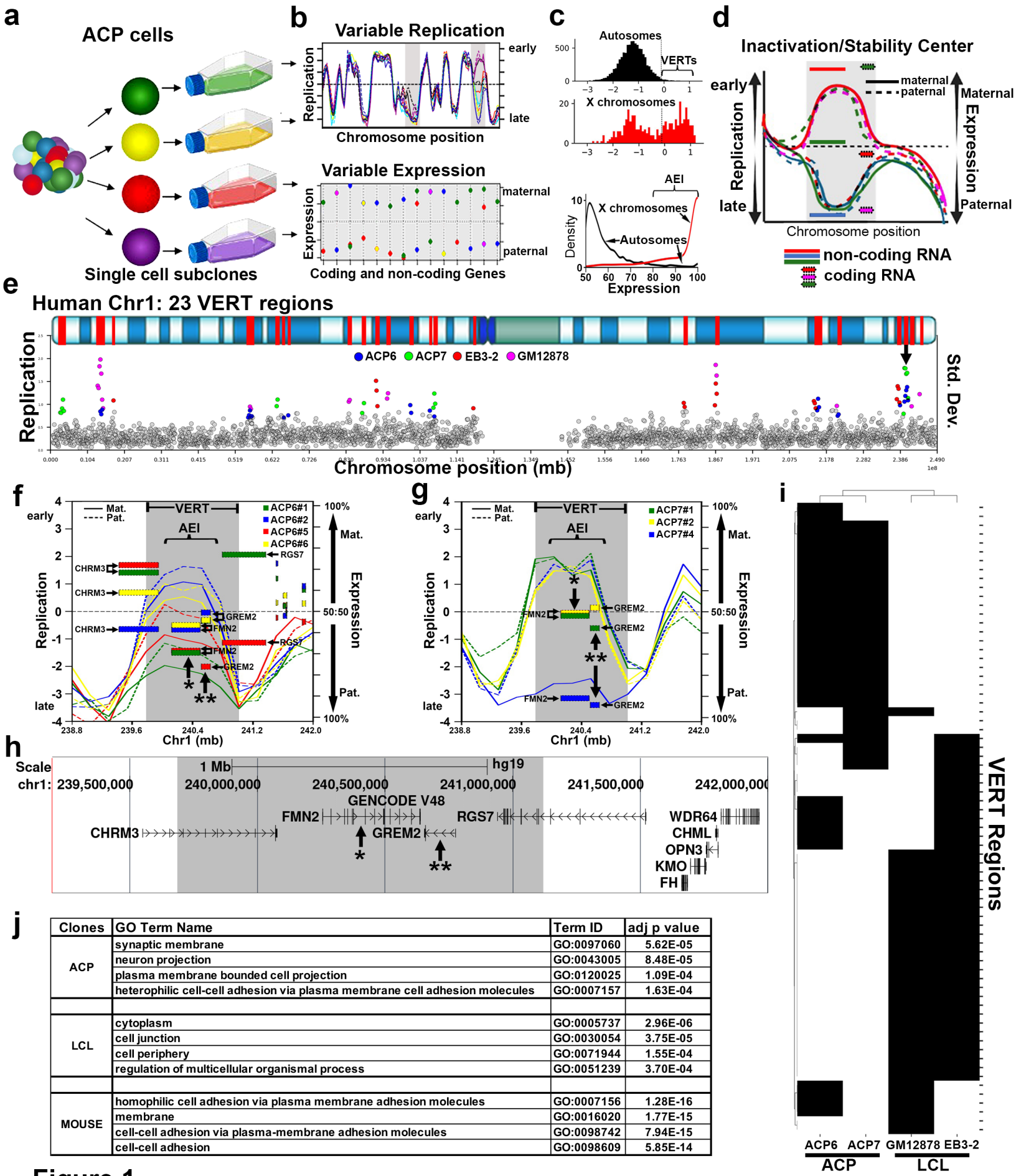

j

Clones	GO Term Name	Term ID	adj p value
ACP	synaptic membrane	GO:0097060	5.62E-05
	neuron projection	GO:0043005	8.48E-05
	plasma membrane bounded cell projection	GO:0120025	1.09E-04
	heterophilic cell-cell adhesion via plasma membrane cell adhesion molecules	GO:0007157	1.63E-04
LCL	cytoplasm	GO:0005737	2.96E-06
	cell junction	GO:0030054	3.75E-05
	cell periphery	GO:0071944	1.55E-04
	regulation of multicellular organismal process	GO:0051239	3.70E-04
MOUSE	homophilic cell adhesion via plasma membrane adhesion molecules	GO:0007156	1.28E-16
	membrane	GO:0016020	1.77E-15
	cell-cell adhesion via plasma-membrane adhesion molecules	GO:0098742	7.94E-15
	cell-cell adhesion	GO:0098609	5.85E-14

Figure 1

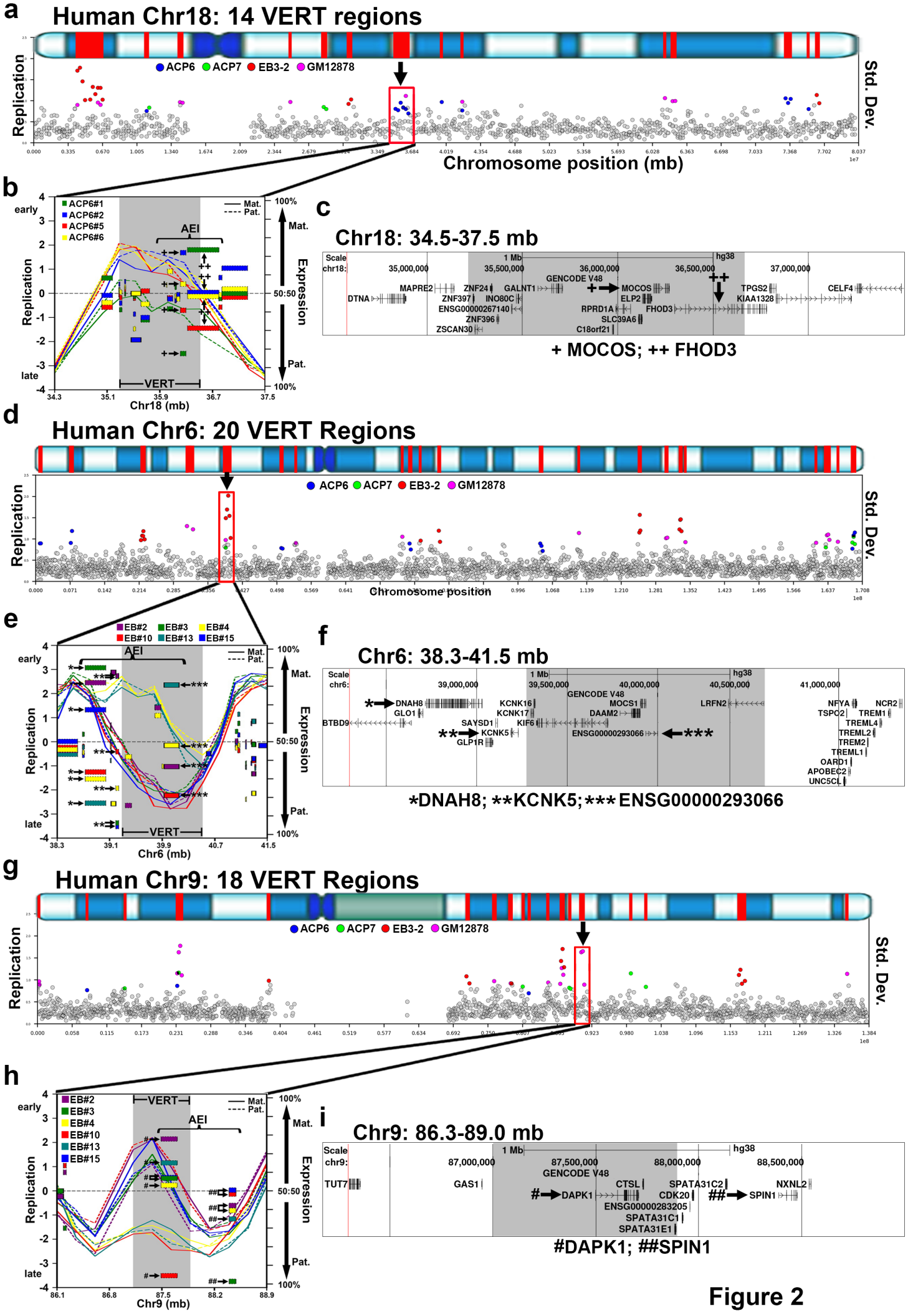
a
Human Chr18: 14 VERT regions
ACP6 ACP7 EB3-2 GM12878
Replication
Std. Dev.
Chromosome position (mb)
b
ACP6#1
ACP6#2
ACP6#5
ACP6#6
Mat.
Pat.
AEI
VERT
early
late
Replication
Expression
100%
50:50
Chr18 (mb)
c
Chr18: 34.5-37.5 mb
Scale
chr18:
1 Mb
hg38
GENCODE V48
DTNA
MAPRE2
ZNF397
ZNF24
INO80C
GALNT1
ENSG00000267140
ZNF396
ZSCAN30
MOCOS
ELP2
RPRD1A
SLC39A6
C18orf21
FHOD3
TPGS2
KIAA1328
CELF4
+ MOCOS; ++ FHOD3
d
Human Chr6: 20 VERT Regions
ACP6 ACP7 EB3-2 GM12878
Replication
Std. Dev.
Chromosome position
e
EB#2
EB#3
EB#4
EB#10
EB#13
EB#15
AEI
VERT
early
late
Replication
Expression
Chr6 (mb)
f
Chr6: 38.3-41.5 mb
Scale
chr6:
1 Mb
hg38
GENCODE V48
DNAH8
GLO1
BTBD9
KCNK16
KCNK17
SAYSD1
KIF6
KCNK5
GLP1R
MOCS1
DAAM2
ENSG00000293066
LRFN2
NFYA
NCR2
TSPC2
TREM1
TREML4
TREML2
TREM2
TREML1
OARD1
APOBEC2
UNC5CL
*DNAH8; **KCNK5; *** ENSG00000293066
g
Human Chr9: 18 VERT Regions
ACP6 ACP7 EB3-2 GM12878
Replication
Std. Dev.
h
EB#2
EB#3
EB#4
EB#10
EB#13
EB#15
VERT
AEI
early
late
Replication
Expression
Chr9 (mb)
i
Chr9: 86.3-89.0 mb
Scale
chr9:
1 Mb
hg38
GENCODE V48
TUT7
GAS1
DAPK1
CTSL
ENSG00000283205
SPATA31C1
SPATA31E1
CDK20
SPATA31C2
SPIN1
NXNL2
#DAPK1; ##SPIN1

Figure 2

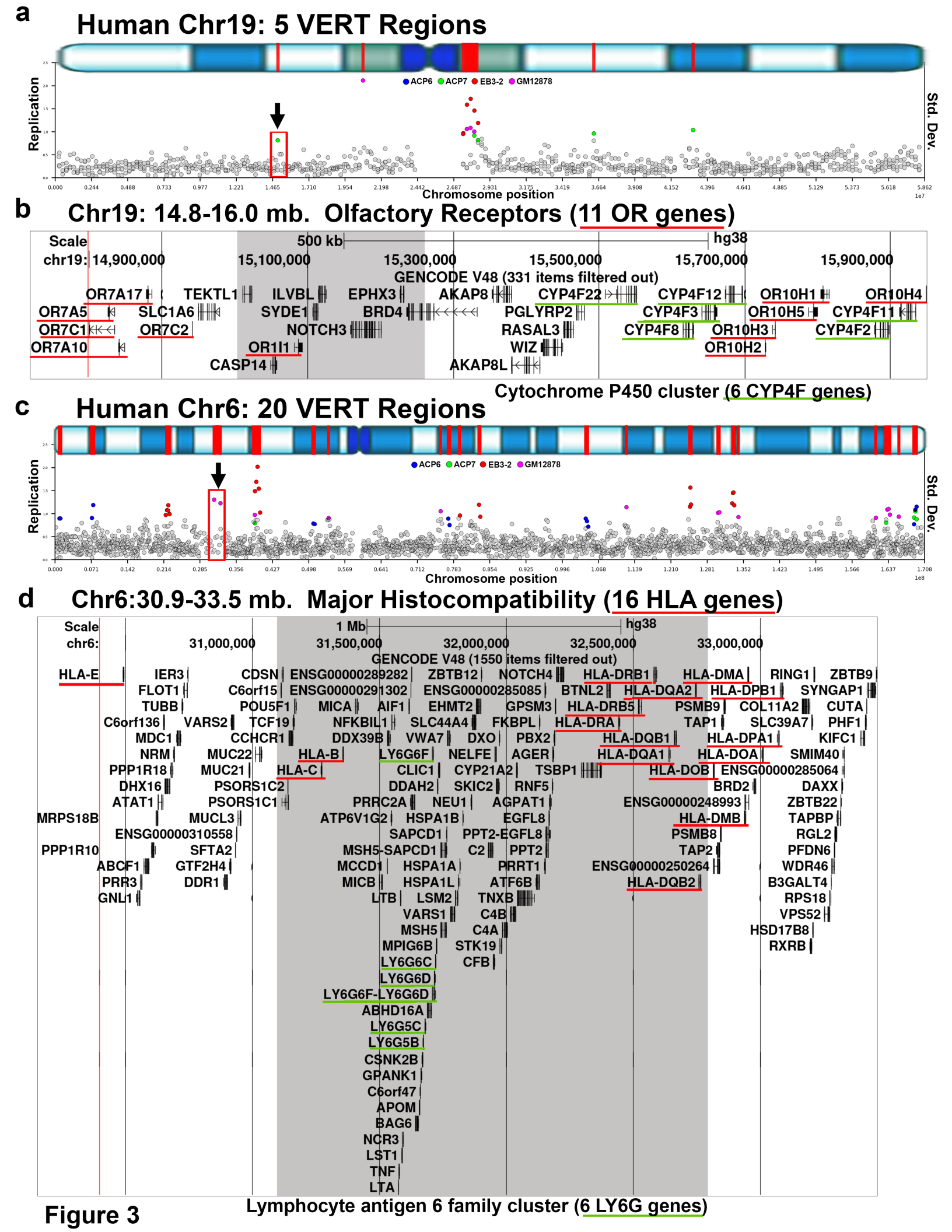
a
Human Chr19: 5 VERT Regions
ACP6 ACP7 EB3-2 GM12878
Replication
Std. Dev.
Chromosome position
b
Chr19: 14.8-16.0 mb. Olfactory Receptors (11 OR genes)
Scale
chr19:
500 kb
hg38
14,900,000
15,100,000
15,300,000
15,500,000
15,700,000
15,900,000
GENCODE V48 (331 items filtered out)
OR7A17
TEKTL1
ILVBL
EPHX3
AKAP8
CYP4F22
CYP4F12
OR10H1
OR10H4
OR7A5
SLC1A6
SYDE1
BRD4
PGLYRP2
CYP4F3
OR10H5
CYP4F11
OR7C1
OR7C2
NOTCH3
RASAL3
CYP4F8
OR10H3
CYP4F2
OR7A10
OR1I1
WIZ
OR10H2
CASP14
AKAP8L
Cytochrome P450 cluster (6 CYP4F genes)
c
Human Chr6: 20 VERT Regions
ACP6 ACP7 EB3-2 GM12878
Replication
Std. Dev.
Chromosome position
d
Chr6:30.9-33.5 mb. Major Histocompatibility (16 HLA genes)
Scale
chr6:
1 Mb
hg38
31,000,000
31,500,000
32,000,000
32,500,000
33,000,000
GENCODE V48 (1550 items filtered out)
HLA-E
IER3
CDSN
ENSG00000289282
ZBTB12
NOTCH4
HLA-DRB1
HLA-DMA
RING1
ZBTB9
FLOT1
C6orf15
ENSG00000291302
ENSG00000285085
BTNL2
HLA-DQA2
HLA-DPB1
SYNGAP1
TUBB
POU5F1
MICA
AIF1
EHMT2
GPSM3
HLA-DRB5
PSMB9
COL11A2
CUTA
C6orf136
VARS2
TCF19
NFKBIL1
SLC44A4
FKBPL
HLA-DRA
TAP1
SLC39A7
PHF1
MDC1
CCHCR1
DDX39B
VWA7
DXO
PBX2
HLA-DQB1
HLA-DPA1
KIFC1
NRM
MUC22
HLA-B
LY6G6F
NELFE
AGER
HLA-DQA1
HLA-DOA
SMIM40
PPP1R18
MUC21
HLA-C
CLIC1
CYP21A2
TSBP1
HLA-DOB
ENSG00000285064
DHX16
PSORS1C2
DDAH2
SKIC2
RNF5
BRD2
DAXX
ATAT1
PSORS1C1
PRRC2A
NEU1
AGPAT1
ENSG00000248993
ZBTB22
MRPS18B
MUCL3
ATP6V1G2
HSPA1B
EGFL8
HLA-DMB
TAPBP
ENSG00000310558
SAPCD1
PPT2-EGFL8
PSMB8
RGL2
PPP1R10
SFTA2
MSH5-SAPCD1
C2
PPT2
TAP2
PFDN6
ABCF1
GTF2H4
MCCD1
HSPA1A
PRRT1
ENSG00000250264
WDR46
PRR3
DDR1
MICB
HSPA1L
ATF6B
HLA-DQB2
B3GALT4
GNL1
LTB
LSM2
TNXB
RPS18
VARS1
C4B
VPS52
MSH5
C4A
HSD17B8
MPIG6B
STK19
RXRB
LY6G6C
CFB
LY6G6D
LY6G6F-LY6G6D
ABHD16A
LY6G5C
LY6G5B
CSNK2B
GPANK1
C6orf47
APOM
BAG6
NCR3
LST1
TNF
LTA
Lymphocyte antigen 6 family cluster (6 LY6G genes)

Figure 3

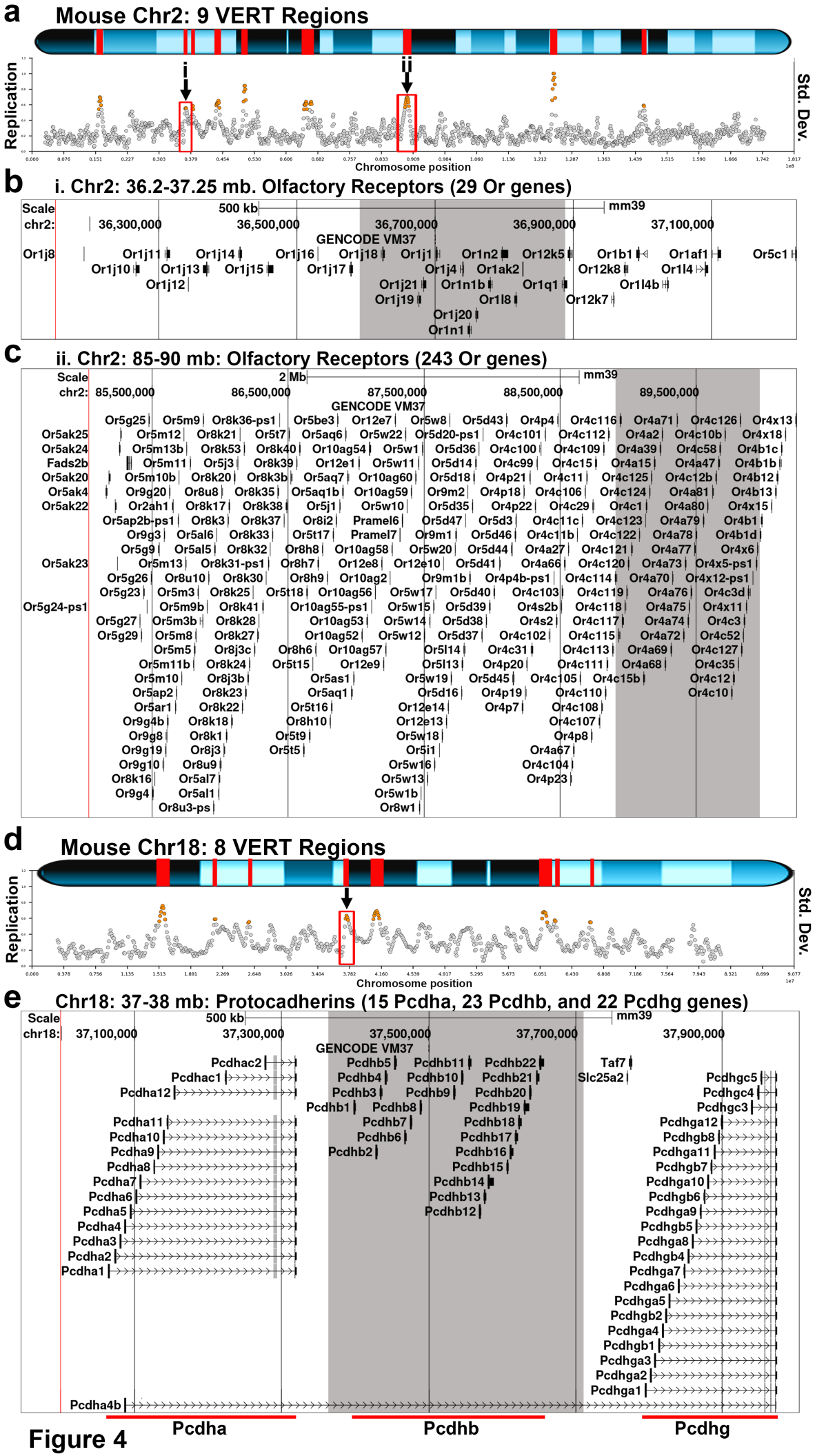
a
Mouse Chr2: 9 VERT Regions
Replication
Std. Dev.
i
ii
Chromosome position
b
i. Chr2: 36.2-37.25 mb. Olfactory Receptors (29 Or genes)
Scale
500 kb
mm39
chr2:
36,300,000
36,500,000
36,700,000
36,900,000
37,100,000
GENCODE VM37
Or1j8
Or1j11
Or1j14
Or1j16
Or1j18
Or1j1
Or1n2
Or12k5
Or1b1
Or1af1
Or5c1
Or1j10
Or1j13
Or1j15
Or1j17
Or1j4
Or1ak2
Or12k8
Or1l4
Or1j12
Or1j21
Or1n1b
Or1q1
Or1l4b
Or1j19
Or1l8
Or12k7
Or1j20
Or1n1
c
ii. Chr2: 85-90 mb: Olfactory Receptors (243 Or genes)
Scale
2 Mb
mm39
chr2:
85,500,000
86,500,000
87,500,000
88,500,000
89,500,000
GENCODE VM37
Or5g25
Or5m9
Or8k36-ps1
Or5be3
Or12e7
Or5w8
Or5d43
Or4p4
Or4c116
Or4a71
Or4c126
Or4x13
Or5ak25
Or5m12
Or8k21
Or5t7
Or5aq6
Or5w22
Or5d20-ps1
Or4c101
Or4c112
Or4a2
Or4c10b
Or4x18
Or5ak24
Or5m13b
Or8k53
Or8k40
Or10ag54
Or5w1
Or5d36
Or4c100
Or4c109
Or4a39
Or4c58
Or4b1c
Fads2b
Or5m11
Or5j3
Or8k39
Or12e1
Or5w11
Or5d14
Or4c99
Or4c15
Or4a15
Or4a47
Or4b1b
Or5ak20
Or5m10b
Or8k20
Or8k3b
Or5aq7
Or10ag60
Or5d18
Or4p21
Or4c11
Or4c125
Or4c12b
Or4b12
Or5ak4
Or9g20
Or8u8
Or8k35
Or5aq1b
Or10ag59
Or9m2
Or4p18
Or4c106
Or4c124
Or4a81
Or4b13
Or5ak22
Or2ah1
Or8k17
Or8k38
Or5j1
Or5w10
Or5d35
Or4p22
Or4c29
Or4c1
Or4a80
Or4x15
Or5ap2b-ps1
Or8k3
Or8k37
Or8i2
Pramel6
Or5d47
Or5d3
Or4c11c
Or4c123
Or4a79
Or4b1
Or9g3
Or5al6
Or8k33
Or5t17
Pramel7
Or9m1
Or5d46
Or4c11b
Or4c122
Or4a78
Or4b1d
Or5g9
Or5al5
Or8k32
Or8h8
Or10ag58
Or5w20
Or5d44
Or4a27
Or4c121
Or4a77
Or4x6
Or5ak23
Or5m13
Or8k31-ps1
Or8h7
Or12e8
Or12e10
Or5d41
Or4a66
Or4c120
Or4a73
Or4x5-ps1
Or5g26
Or8u10
Or8k30
Or8h9
Or10ag2
Or9m1b
Or4p4b-ps1
Or4c114
Or4a70
Or4x12-ps1
Or5g23
Or5m3
Or8k25
Or5t18
Or10ag56
Or5w17
Or5d40
Or4c103
Or4c119
Or4a76
Or4c3d
Or5g24-ps1
Or5m9b
Or8k41
Or10ag55-ps1
Or5w15
Or5d39
Or4s2b
Or4c118
Or4a75
Or4x11
Or5g27
Or5m3b
Or8k28
Or10ag53
Or5w14
Or5d38
Or4s2
Or4c117
Or4a74
Or4c3
Or5g29
Or5m8
Or8k27
Or10ag52
Or5w12
Or5d37
Or4c102
Or4c115
Or4a72
Or4c52
Or5m5
Or8j3c
Or8h6
Or10ag57
Or5l14
Or4c31
Or4c113
Or4a69
Or4c127
Or5m11b
Or8k24
Or5t15
Or12e9
Or5l13
Or4p20
Or4c111
Or4a68
Or4c35
Or5m10
Or8j3b
Or5as1
Or5w19
Or5d45
Or4c105
Or4c15b
Or4c12
Or5ap2
Or8k23
Or5aq1
Or5d16
Or4p19
Or4c110
Or4c10
Or5ar1
Or8k22
Or5t16
Or12e14
Or4p7
Or4c108
Or9g4b
Or8k18
Or8h10
Or12e13
Or4c107
Or9g8
Or8k1
Or5t9
Or5w18
Or4p8
Or9g19
Or8j3
Or5t5
Or5i1
Or4a67
Or9g10
Or8u9
Or5w16
Or4c104
Or8k16
Or5al7
Or5w13
Or4p23
Or9g4
Or5al1
Or5w1b
Or8u3-ps
Or8w1
d
Mouse Chr18: 8 VERT Regions
Replication
Std. Dev.
Chromosome position
e
Chr18: 37-38 mb: Protocadherins (15 Pcdha, 23 Pcdhb, and 22 Pcdhg genes)
Scale
500 kb
mm39
chr18:
37,100,000
37,300,000
37,500,000
37,700,000
37,900,000
GENCODE VM37
Pcdhac2
Pcdhac1
Pcdha12
Pcdha11
Pcdha10
Pcdha9
Pcdha8
Pcdha7
Pcdha6
Pcdha5
Pcdha4
Pcdha3
Pcdha2
Pcdha1
Pcdhb5
Pcdhb11
Pcdhb22
Pcdhb4
Pcdhb10
Pcdhb21
Pcdhb3
Pcdhb9
Pcdhb20
Pcdhb1
Pcdhb8
Pcdhb19
Pcdhb7
Pcdhb18
Pcdhb6
Pcdhb17
Pcdhb2
Pcdhb16
Pcdhb15
Pcdhb14
Pcdhb13
Pcdhb12
Taf7
Slc25a2
Pcdhgc5
Pcdhgc4
Pcdhgc3
Pcdhga12
Pcdhgb8
Pcdhga11
Pcdhgb7
Pcdhga10
Pcdhgb6
Pcdhga9
Pcdhgb5
Pcdhga8
Pcdhgb4
Pcdhga7
Pcdhga6
Pcdhga5
Pcdhgb2
Pcdhga4
Pcdhgb1
Pcdhga3
Pcdhga2
Pcdhga1
Pcdha4b
Pcdha
Pcdhb
Pcdhg

Figure 4

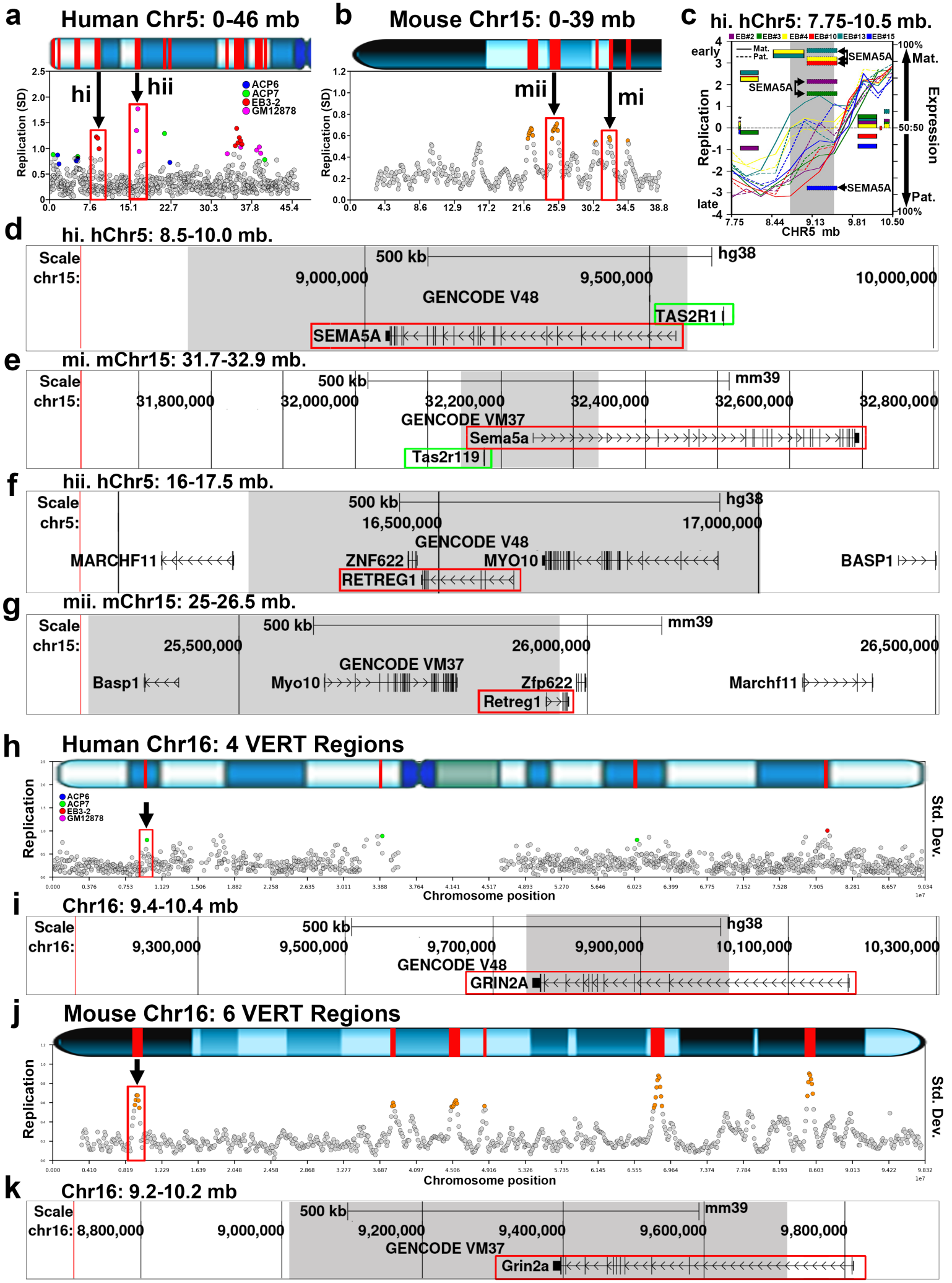
a
Human Chr5: 0-46 mb
hi
hii
ACP6
ACP7
EB3-2
GM12878
Replication (SD)
b
Mouse Chr15: 0-39 mb
mii
mi
Replication (SD)
c
hi. hChr5: 7.75-10.5 mb.
EB#2 EB#3 EB#4 EB#10 EB#13 EB#15
Mat.
Pat.
early
late
SEMA5A
Replication
Expression
100%
Mat.
50:50
Pat.
CHR5 mb
d
hi. hChr5: 8.5-10.0 mb.
Scale
chr15:
500 kb
hg38
9,000,000
9,500,000
10,000,000
GENCODE V48
TAS2R1
SEMA5A
e
mi. mChr15: 31.7-32.9 mb.
Scale
chr15:
500 kb
mm39
31,800,000
32,000,000
32,200,000
32,400,000
32,600,000
32,800,000
GENCODE VM37
Sema5a
Tas2r119
f
hii. hChr5: 16-17.5 mb.
Scale
chr5:
500 kb
hg38
16,500,000
17,000,000
GENCODE V48
MARCHF11
ZNF622
MYO10
BASP1
RETREG1
g
mii. mChr15: 25-26.5 mb.
Scale
chr15:
500 kb
mm39
25,500,000
26,000,000
26,500,000
GENCODE VM37
Basp1
Myo10
Zfp622
Marchf11
Retreg1
h
Human Chr16: 4 VERT Regions
ACP6
ACP7
EB3-2
GM12878
Replication
Std. Dev.
Chromosome position
i
Chr16: 9.4-10.4 mb
Scale
chr16:
500 kb
hg38
9,300,000
9,500,000
9,700,000
9,900,000
10,100,000
10,300,000
GENCODE V48
GRIN2A
j
Mouse Chr16: 6 VERT Regions
Replication
Std. Dev.
Chromosome position
k
Chr16: 9.2-10.2 mb
Scale
chr16:
500 kb
mm39
8,800,000
9,000,000
9,200,000
9,400,000
9,600,000
9,800,000
GENCODE VM37
Grin2a

Figure 5

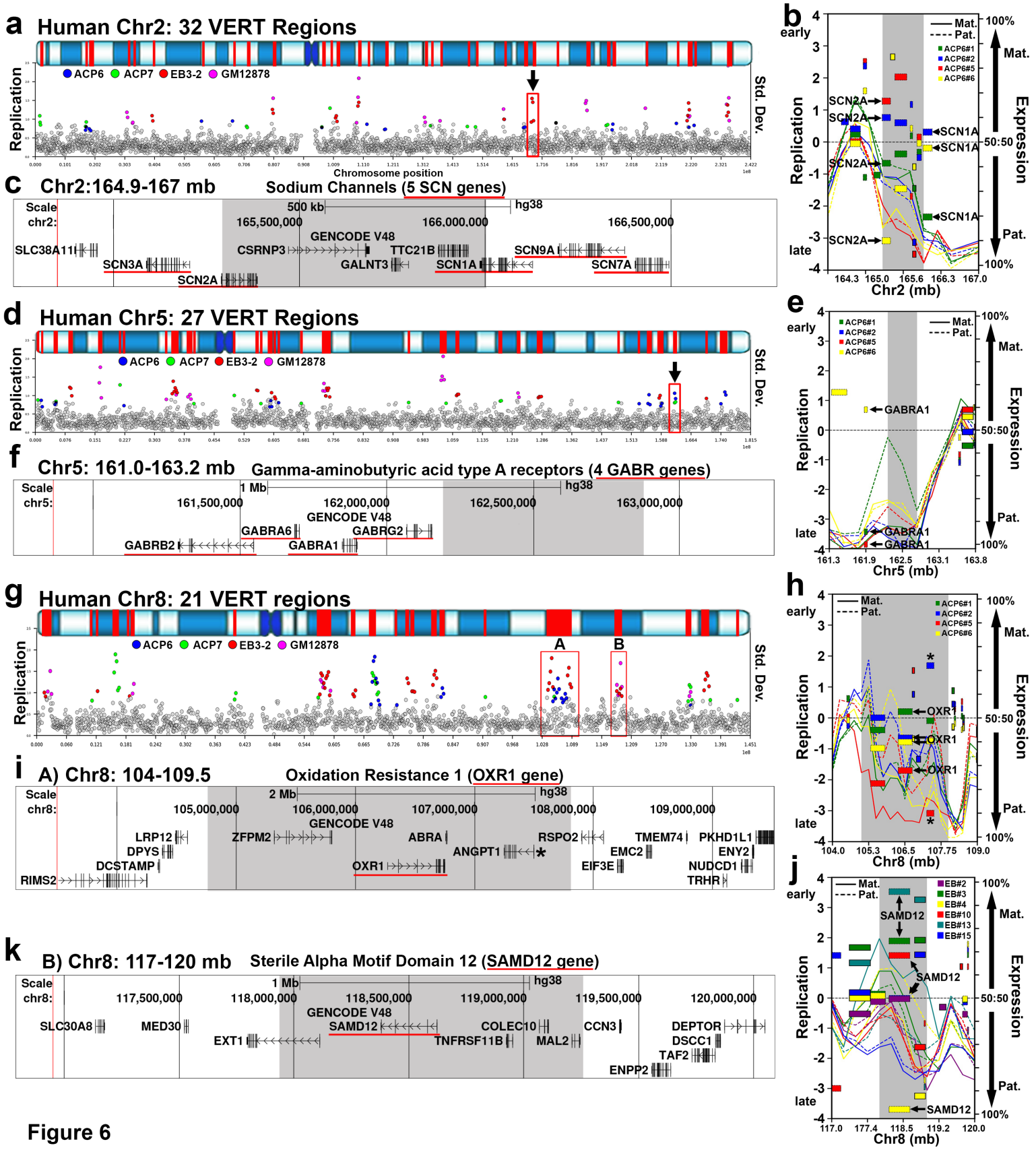
a
Human Chr2: 32 VERT Regions
ACP6 ACP7 EB3-2 GM12878
Replication
Std. Dev.
Chromosome position
b
early
late
Mat.
Pat.
ACP6#1
ACP6#2
ACP6#5
ACP6#6
SCN2A
SCN1A
Replication
Expression
100%
50:50
Chr2 (mb)
c
Chr2:164.9-167 mb
Sodium Channels (5 SCN genes)
Scale
chr2:
500 kb
hg38
165,500,000
166,000,000
166,500,000
GENCODE V48
SLC38A11
SCN3A
SCN2A
CSRNP3
GALNT3
TTC21B
SCN1A
SCN9A
SCN7A
d
Human Chr5: 27 VERT Regions
ACP6 ACP7 EB3-2 GM12878
Replication
Std. Dev.
e
GABRA1
Chr5 (mb)
f
Chr5: 161.0-163.2 mb
Gamma-aminobutyric acid type A receptors (4 GABR genes)
Scale
chr5:
1 Mb
hg38
161,500,000
162,000,000
162,500,000
163,000,000
GENCODE V48
GABRB2
GABRA6
GABRA1
GABRG2
g
Human Chr8: 21 VERT regions
ACP6 ACP7 EB3-2 GM12878
A
B
Replication
Std. Dev.
h
OXR1
Chr8 (mb)
i
A) Chr8: 104-109.5
Oxidation Resistance 1 (OXR1 gene)
Scale
chr8:
2 Mb
hg38
105,000,000
106,000,000
107,000,000
108,000,000
109,000,000
GENCODE V48
LRP12
DPYS
DCSTAMP
RIMS2
ZFPM2
ABRA
ANGPT1
OXR1
RSPO2
EMC2
EIF3E
TMEM74
PKHD1L1
ENY2
NUDCD1
TRHR
j
SAMD12
Chr8 (mb)
k
B) Chr8: 117-120 mb
Sterile Alpha Motif Domain 12 (SAMD12 gene)
Scale
chr8:
1 Mb
hg38
117,500,000
118,000,000
118,500,000
119,000,000
119,500,000
120,000,000
GENCODE V48
SLC30A8
MED30
EXT1
SAMD12
TNFRSF11B
COLEC10
MAL2
CCN3
DEPTOR
DSCC1
TAF2
ENPP2

Figure 6

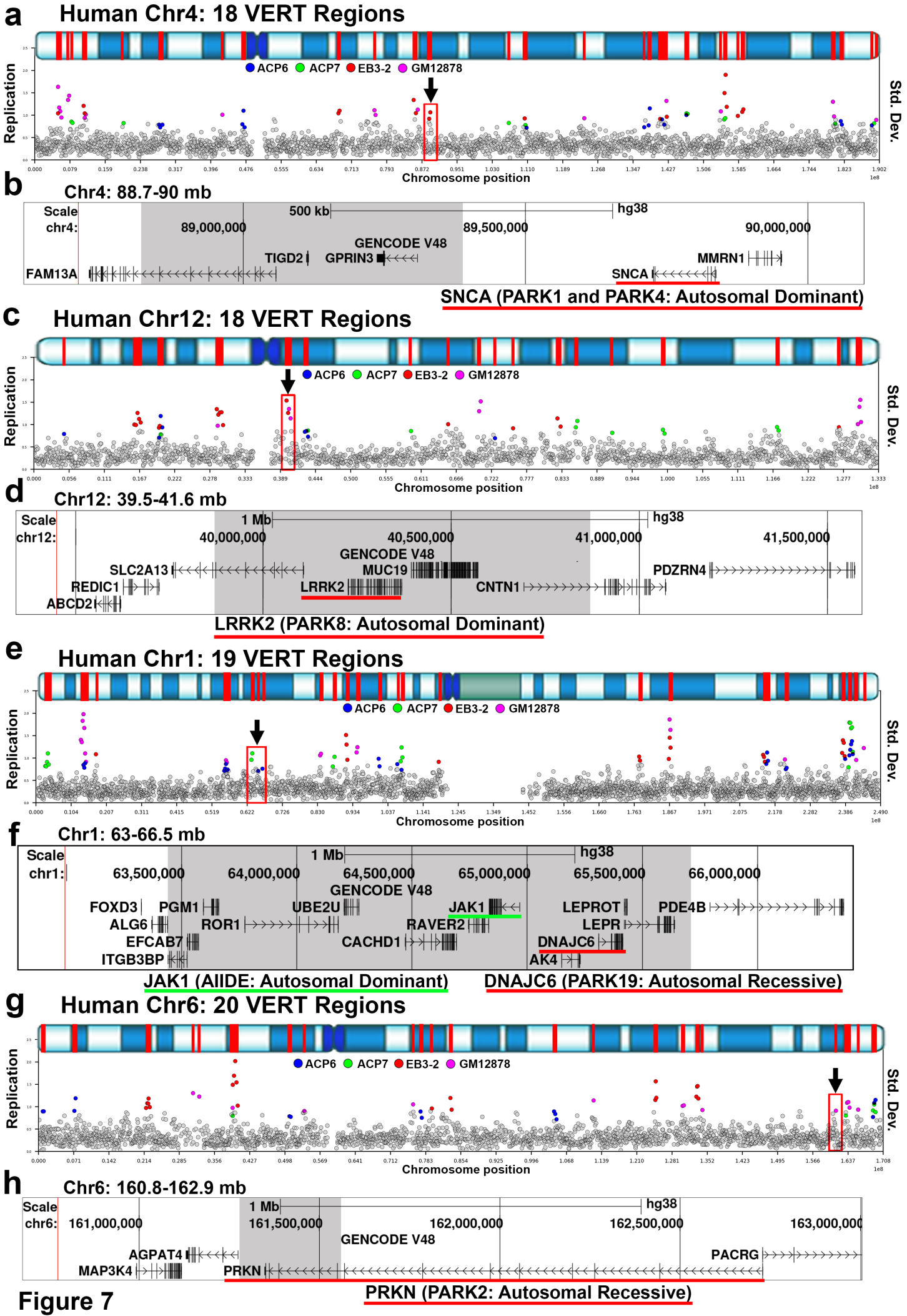
a
Human Chr4: 18 VERT Regions
ACP6 ACP7 EB3-2 GM12878
Replication
Std. Dev.
Chromosome position
b
Chr4: 88.7-90 mb
Scale
chr4:
500 kb
hg38
89,000,000
89,500,000
90,000,000
GENCODE V48
TIGD2
GPRIN3
MMRN1
FAM13A
SNCA
SNCA (PARK1 and PARK4: Autosomal Dominant)
c
Human Chr12: 18 VERT Regions
ACP6 ACP7 EB3-2 GM12878
Replication
Std. Dev.
Chromosome position
d
Chr12: 39.5-41.6 mb
Scale
chr12:
1 Mb
hg38
40,000,000
40,500,000
41,000,000
41,500,000
GENCODE V48
SLC2A13
MUC19
PDZRN4
REDIC1
LRRK2
CNTN1
ABCD2
LRRK2 (PARK8: Autosomal Dominant)
e
Human Chr1: 19 VERT Regions
ACP6 ACP7 EB3-2 GM12878
Replication
Std. Dev.
Chromosome position
f
Chr1: 63-66.5 mb
Scale
chr1:
1 Mb
hg38
63,500,000
64,000,000
64,500,000
65,000,000
65,500,000
66,000,000
GENCODE V48
FOXD3
PGM1
UBE2U
JAK1
LEPROT
PDE4B
ALG6
ROR1
RAVER2
LEPR
EFCAB7
CACHD1
DNAJC6
ITGB3BP
AK4
JAK1 (AIIDE: Autosomal Dominant)
DNAJC6 (PARK19: Autosomal Recessive)
g
Human Chr6: 20 VERT Regions
ACP6 ACP7 EB3-2 GM12878
Replication
Std. Dev.
Chromosome position
h
Chr6: 160.8-162.9 mb
Scale
chr6:
1 Mb
hg38
161,000,000
161,500,000
162,000,000
162,500,000
163,000,000
GENCODE V48
AGPAT4
PACRG
MAP3K4
PRKN
PRKN (PARK2: Autosomal Recessive)

Figure 7